Langmuir

Article

pubs.acs.org/Langmuir

Pyrenyl-Linker-Glucono Gelators. Correlations of Gel Properties with Gelator Structures and Characterization of Solvent Effects

Ni Yan,[†,‡] Zhiyan Xu,[†] Kevin K. Diehn,[§] Srinivasa R. Raghavan,[§] Yu Fang,*[,†] and Richard G. Weiss*[,‡]

[†]Key Laboratory of Applied Surface and Colloid Chemistry (Ministry of Education), School of Chemistry and Chemical Engineering, Shaanxi Normal University, Xi'an 710062, P. R. China

[‡]Department of Chemistry, Georgetown University, Washington, DC 20057-1227, United States

[§]Department of Chemical and Biomolecular Engineering, University of Maryland, College Park, Maryland 20742-2111, United States

Supporting Information

ABSTRACT: A series of glucono-appended 1-pyrenesulfonyl derivatives containing α,ω-diaminoalkane spacers (**P***n*, where *n*, the number of methylene units separating the amino groups, is 2, 3, 4, 6, 7, and 8) have been prepared. Careful analyses of correlations between the structures of these molecules and their gels have provided important insights into the factors responsible for one-dimensional aggregation of small molecules containing both lipophilic and hydrophilic parts. The gelation behavior has been examined in 30 liquids of diverse structure and polarity, and the properties of their gels and the gelation mechanisms have been investigated using a variety of techniques. Possible reasons are discussed regarding why the **P***n* are better gelators than the corresponding naphthyl analogues (**N***n*) which had been investigated previously. **P2** and **P3** are ambidextrous gelators (i.e., they gelate both water and some organic liquids), and **P4**−**P8** gelate some organic liquids which are protic and aprotic, but not water. In at least one of the liquids examined, **P3**, **P4**, **P6**, **P7**, and **P8** form gels at less than 1 w/v % concentrations, and some of the gels in 1-decanol are thixotropic. Analyses of the gelation abilities using Hansen solubility parameters yield both qualitative and quantitative insights into the role of liquid-gelator interactions. For example, the critical gelation concentrations increase generally with increasing polar and hydrogen bonding interactions between the gelators and their liquid components. As revealed by FT-IR, ^{1}H NMR, UV−vis, and fluorescence spectra, hydrogen-bonding between glucono units and $\pi-\pi$ stacking between pyrenyl groups are important in the formation and maintenance of the gel networks. The results from this study, especially those relating the aggregation modes and liquid properties, offer insights for the design of new surfactant-containing low-molecular-mass gelators with predefined gelating abilities.

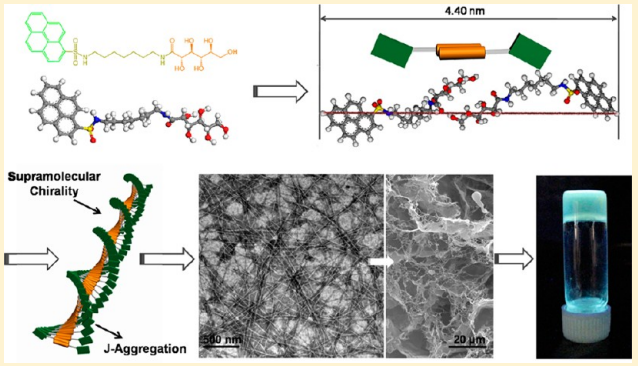

INTRODUCTION

Gels consisting of a low concentration of a low-molecular-mass gelator (LMOG) and a liquid, as well as the mechanisms of their formation, are receiving increased attention because of the many realized and potential applications of these materials[1−3] and because of the insights into one-dimensional (1D) aggregation and self-assembly modes that they provide.[4,5] Solutions/sols of LMOGs can self-assemble[6] into 1D fibers, rods, ribbons, and nanotubes, as well as two-dimensional (2D) objects (i.e., platelets) or other aggregate morphologies through hydrogen bonding, $\pi-\pi$ stacking, London dispersion forces, and other types of van der Waals interactions. A key requirement for these objects to make gels is their additional organization into three-dimensional (3D) networks which can immobilize the liquid component.[4] Because the noncovalent forces responsible for the 1D objects and their 3D networks are intrinsically weaker than the covalent bonds associated with gels based on cross-linked polymeric networks, LMOG-based gels are, in general, more responsive to stimuli such as heat, light,[7] ultrasound,[8] shearing,[9] pH,[10] host−guest complexes,[11] added metallic ions,[12] and oxidative/reductive reactions.[9] Examples of each of these have been documented to influence the strengths of LMOG gels and their sol−gel transitions.

Gelation of liquids by LMOGs requires a fine balance between dissolution and aggregation.[13] Many LMOG molecules contain functional groups which promote both tendencies in a given liquid. For example, we and others have explored the gelating abilities of LMOGs, which consist of an aromatic group (A), a linker (L), and a steroidal (S) group.[14] Even when very intriguing differences in the modes of aggregation and gelation of the ALS molecules have been identified to be a consequence of subtle changes in the liquid component,[15] the underlying physical causes have been difficult to separate.

Some members of another class of LMOGs, amphiphiles in which the A[16,17] (or a long alkyl chain[1,18]) and L parts are

Received: December 16, 2012
Published: December 19, 2012

retained, but the steroidal group has been replaced by a carbohydrate-based species, have been found capable of gelating both water and organic liquids: they are ambidextrous. In water, their hydrophobic groups promote aggregation and hydrophilic groups provide solubility; in organic liquids, aggregation is driven by the hydrophilic groups and dissolution by the hydrophobic ones. Again, these trends are only qualitative—the degree to which each factor affects gelation is not known and there is no set of "rules" to determine a priori when a liquid will be gelated by a specific LMOG and how strong and stable the gels will be. Thus, structure−gelation relationships in this field are sorely needed. An approach to achieving such relationships is to examine the gelating properties of series of structurally related molecules in a wide range of liquid types.

Previously, we employed 2-naphthyl as a hydrophobic group and glucono as a hydrophilic moiety, separated by α,ω-diamine spacers of different lengths, to prepare a series of fluorescent LMOGs (**N*n***, Chart 1).[19] The **N*n*** with shorter spacers were

Chart 1. Molecular Structures of the Glucono-Based 1-Pyrenyl Derivatives (P*n* where *n* = 2, 3, 4, 6, 7, 8) and 2-Naphthyl Derivatives (N*n* where *n* = 0, 2, 3, 4, 6)

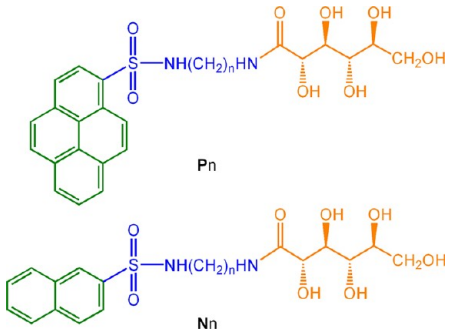

hydrogelators, ambidextrous with somewhat longer spacers, and organogelators with the longest spacers. An advantage of such LMOGs is that changes in the fluorescence spectra[20] and intensities[21] from the aromatic groups can be diagnostics for the degree of aggregation and progress toward gelation (i.e., gel-to-sol or sol-to-gel phase transitions) as well as for the nature of the organization within the assembled objects.[15,22]

The role of the properties of the other key component of a gel, the liquid, is not well understood either. However, Hansen solubility parameters (HSPs) have been used for several decades to select appropriate solvents for polymers.[23] In this method, the overall energy density (δ) is separated into dispersive (δ_d), polar (δ_p), and hydrogen-bonding (δ_h) interaction components (eq 1). Recently, HSPs have shown promise to understand the relationship between the properties needed in an LMOG and a liquid if gelation is to be achieved.[24−26]

$$\delta = \sqrt{{\delta_d}^2 + {\delta_p}^2 + {\delta_h}^2} \quad (1)$$

In addition, we investigated the consequences of substituting a 1-pyrenyl group for the 2-naphthyl group in **N3**, yielding **P3** (Chart 1).[27] Those results indicated that the pyrenyl series of gelators, **P*n***, might be more efficient gelators and offer other advantages for analytical studies over the **N*n***.[27] In order to extend the comparisons among LMOGs of similar structures and to quantify further the interactions among them with different liquids, we examine here: (1) the gelating ability of a series of **P*n*** LMOGs in which the spacers between the pyrenyl and glucono groups have been varied; (2) the properties of their gels in a wide range of liquids; and (3) correlations between the Hansen solubility parameters and the gelation trends of the **P*n***.

Substitution of 1-pyrenyl for 2-naphthyl is not a trivial structural modification because the area and volume occupied by pyrene (187.04 Å^2 and 181.13 Å^3, respectively), being significantly larger than that of naphthalene (139.87 Å^2 and 123.99 Å^3, respectively),[28] can affect in a significant way how the gelator molecules pack into the objects that evolve into the 3D gelator networks. Furthermore, pyrenyl moieties have much higher fluorescence quantum yields than their naphthyl counterparts and they are more prone to form detectable excimers. These attributes allow more detailed insights into the molecular packing arrangements within the gel matrixes than are available with the **N*n***. In fact, the results presented here demonstrate that the **P*n*** are much more efficient LMOGs than the **N*n***[19] (as measured by several experimental criteria) and their gels behave in very different ways. The insights derived from those results have led to a deeper understanding of the LMOG structure−gelation and LMOG−liquid relationships.

EXPERIMENTAL SECTION

Syntheses and Purifications of P*n*. Details concerning the syntheses and purification of the **P*n*** are included in Supporting Information. The initially purified material, referred to as Series A, was used in all experiments except as noted in the text. In some experiments, Series A material was purified further to yield **P*n*** denoted as Series B.

Gelation Tests. All concentrations are expressed in % as 100 × the ratio of gelator weight (g) to liquid volume (mL). A known weight of a **P*n*** and a measured volume of selected liquid were placed into a flame-sealed tube (5 mm i.d.), and the tube was heated in an oil bath until the solid was dissolved. After the solution/sol had cooled to room temperature in air, the tube was inverted to determine whether the sample flowed perceptibly. If none was observed over a period of ca. 10 s, the sample was given a preliminary designation of a gel (G). Samples with both a liquid and gel-like material are referred to as partial gels (PG). Samples in which the **P*n*** remained dissolved are solutions or sols (S). When a solid appeared after the **P*n*** dissolved in a hot liquid, the designation given is precipitate (P). If a **P*n*** could not be dissolved even at the boiling point of a liquid, the sample is designated as insoluble (I). Samples with microcrystalline **P*n***, and which flowed when inverted, are designated as suspensions (Sus). Critical gelator concentrations (CGCs) are the lowest **P*n*** concentrations which produced gels (as prepared by the method above). Gelation temperatures (T_{gel}) are the ranges over which gels, inverted in flame-sealed tubes, fell under the influence of gravity when heated at ca. 2 °C/min in a water bath.[29]

Calculation of HSPs. HSP values for the liquids examined were taken from the literature.[23] Hansen space was calculated using version 1.3 of the Hansen Solubility Data Fitting Software from UMD Complex Fluids and Nanomaterials Lab.[30] For the purpose of this analysis, the samples of the **P*n*** in liquids are separated into soluble (S), gel (G), and insoluble (I) categories; suspensions, partial gels, and precipitates were treated as "insoluble". Gels and partial gels formed only under sonication (G* and PG*) were treated as "insoluble" because their mixtures could not be dissolved by heating. HSP values for each gelator were determined using data fitting of each Hansen space. The distances (R_a) between the gelator δ_p, δ_h, and δ_d values and those of a liquid (δ_{ps}, δ_{hs}, and δ_{ds}) in Hansen space were calculated using eq 2.

$$R_a = \sqrt{4(\delta_d - \delta_{ds})^2 + (\delta_p - \delta_{ps})^2 + (\delta_h - \delta_{hs})^2} \quad (2)$$

dx.doi.org/10.1021/la304957n | *Langmuir* 2013, 29, 793−805

Table 1. Appearances,[a] T_{gel} Values (°C) of Gels of 2.5% P*n*, and Critical Gelator Concentrations (CGCs, %) in Different Liquids As Determined in 5 mm (i.d.) Sealed Tubes[d]

liquid	P2	P3[e]	P4	P6	P7	P8
DMSO	S	S	S	S	S	S
DMF	S	S	S	S	S	S
pyridine	S	S	S	S	S	S
n-butylamine	S	S	S	S	S	S
methanol	P[a]	TG 55–56, 0.83	TG[b] 49–50, 1.25	TG[b] 50–51, 0.71	TG 56–57, 0.62	TG[b] 52–53, 1.25
ethanol	P	OG 68–69, 0.83	OG 66–67, 0.5	TG 63–64, 0.62	OG 67–68, 0.42	OG 64–65, 0.56
1-propanol	P	OG 69–70, 0.5	OG 74–75, 0.42	OG[b] 74–75, 0.62	OG 73–74, 0.62	OG[b] 66–67, 0.56
1-butanol	OG 77–78	OG 75–76, 0.09	OG 73–74, 0.31	OG[b] 76–77, 0.83	OG 71–72, 0.36	OG 69–70, 1.25
1-pentanol	OG 82–83	OG 84–85, 0.42	OG 80–81, 0.25	OG 82–83, 0.5	OG 78–79, 0.62	OG[b] 78–79, 0.62
1-hexanol	OG 76–77	OG 89–90, 0.2	OG 88–89, 0.71	OG 90–91, 0.42	TG 86–87, 0.5	OG 90–91, 0.45
1-heptanol	OG	OG 0.08	OG 0.31	OG 0.36	OG 0.42	OG[b] 0.45
1-octanol	OG 83–84	OG 92–93, 0.42	OG[b] 94–95, 0.71	OG 95–96, 0.36	OG 94–95, 0.62	OG[b] 85–86, 0.62
1-nonanol	OG 80–81	OG 100–101, 0.71	OG 97–98, 1.25	OG 96–97, 0.15	OG[c] 98–99, 0.5	OG[c] 88–89, 0.42
1-decanol	OG 74–75	OG[c] 104–105, 0.07	OG[b,c] 83–84, 0.15	OG[b,c] 85–86, 0.3	OG[c] 102–103, 0.2	OG[c] 92–93, 0.3
water	OG 49–50	OG 61–62, 1.25	Sus	Sus	Sus	Sus
acetonitrile	I	I	OG 74–75, 1.0	OG[b] 83–84, 0.09	OG 86–87, 0.08	OG[b] 80–81, 0.42
tetrahydrofuran	I	I	OG[b] 54–55, 0.50	OG 58–59, 0.62	OG 61–62, 0.83	OG[b] 56–57, 0.83
acetone	I	I	TG[b] 57–58, 0.83	TG[b] 59–60, 0.62	OG 74–75, 0.5	OG 66–67, 0.83
ethyl acetate	I	I	OG 80–81, 0.5	TG 89–90, 0.5	TG86–87, 0.08	OG[b] 89–90, 0.09
benzene	I	I	PG[b]	OG[b]	I	I
toluene	I	I	PG[b]	OG[b]	I	I
acetic acid	OG[b]	P	S	S	S	S
hexanoic acid	OG	OG	PG	OG[b]	OG	P
triethylamine	I	I	PG[b]	OG[b]	I	PG[b]
CH_2Cl_2	I	I	PG[b]	I	I	OG[b]
$CHCl_3$	I	I	PG[b]	OG[b]	PG[b]	I
CCl_4	I	I	I	I	I	I
cyclohexane	I	I	I	I	I	I
n-nonane	I	I	I	I	I	I
diethyl ether	I	I	I	I	I	I

[a]OG = opaque gel, TG = transparent gel, PG = partial gel, S = solution, Sus = suspension, P = precipitate, I = insoluble. [b]Gel formation after sonication at room temperature. [c]Thixotropic gel. [d]The same appearances were noted for samples in 1 cm (i.d.) tubes. [e]Appearances cited from ref 27.

Scanning Electron Microscopy (SEM), Transmission Electronic Microscopy (TEM), and Polarizing Optical Microscopy (POM). SEM pictures of xerogels were taken on a Quanta 200 scanning electron microscopy spectrometer (Philips-FEI) at 20 kV and 10 mA. Xerogels were prepared by freeze–drying 2.0% gels. Prior to examination, the xerogel was attached to a copper holder with conductive adhesive tape, and then it was sputter-coated with a thin layer of gold using a SCD 005 cool sputter coater (Bal-Tec) at 30 mA and ∼10 Pa for 80 s. In the following measurements, "freeze–dried" means that samples were prepared in an Alpha1–2 freeze–dryer (Christ) at −80 °C and ∼4 Pa for 24 h.

Samples for TEM measurements were prepared by placing one drop of a 0.02% or 0.05% solution/sol of **P7** in acetonitrile onto a carbon-coated copper grid (400 mesh) and then allowing the liquid to evaporate in air at room temperature. After drying of the grid, the sample was stained with a solution of 2% phosphotungstic acid in ethanol for 1 min and then dried in air. Measurements were made on a JEM-2100 (JEOL) microscope at 200 keV.

POMs were recorded on a Leitz 585 SM-LUX-POL microscope equipped with crossed polars, a Leitz 350 heating stage, a Photometrics CCD camera interfaced to a computer, and an Omega HH503 microprocessor thermometer connected to a J-K-T thermocouple. Samples were flame-sealed in 0.4 or 0.5 mm path-length, flattened Pyrex capillary tubes (VitroCom, Inc.).

Contact Angles. Static contact angle measurements were performed on an OCA 20 video-based contact angle measuring device (Data-Physics). A drop of a hot solution/sol was placed onto a mica sheet, cooled to room temperature (to form a gel), and freeze–dried. Water droplets were placed on the freeze–dried surface via a microsyringe, and images were captured to measure the angle of the liquid–solid interface. Each sample was recorded at six different points on a surface.

Steady-State Fluorescence. Steady-state emission spectra of the gel and sol phases of N_2-saturated 1.5% **P7** (Series B) in acetonitrile in flame-sealed 4 mm (width) × 7 mm (length) Pyrex flattened capillaries (VitroCom, Inc.) were recorded in a front-face mode at an angle of ∼45° with respect to the incident beam of a Photon Technology International Fluorometer (SYS 2459). In order to compare the change in the fluorescence spectra with gelation, a sample was heated and cooled using a Quantumwest temperature controller and an Omega temperature probe at ca. 10 °C/min, allowing 20 min equilibration time before recording spectra. The sample was not moved between recording spectra at different temperatures, and the instrumental parameters were unchanged.

NMR. ^{1}H and ^{13}C NMR spectra were recorded on an AVANCE 300 MHz spectrometer (Bruker). Data processing and analyses were performed using *MestRe-C 2.3a* software. Chemical shifts were referenced to an internal standard, tetramethylsilane (TMS).

FTIR. Spectra of sols and gels were recorded in transmission mode using a Bruker Equinox 55 infrared spectrometer. The gel samples were coated onto a KBr plate as a smooth film and then freeze–dried. Drops of hot sol samples were dropped onto a KBr plate and then freeze–dried as described above.

Elemental Analyses. Analysis was performed on a Perkin-Elmer 2400 CHN elemental analyzer using acetanilide as a calibration standard.

dx.doi.org/10.1021/la304957n | *Langmuir* 2013, 29, 793–805

X-ray Diffraction (XRD) and Calculated Molecular Lengths. The XRD diffractogram of a xerogel from 2% **P7** (Series B) in acetonitrile was collected on a D/Max-2550/PC diffractometer with Cu Kα (λ = 0.154 nm) radiation generated at 40 kV and 40 mA. The scan rate was 1°/min. The xerogel was prepared by placing an aliquot of a gel directly onto a glass sample holder which was then freeze–dried as described above. XRD diffractograms of neat powders, neat liquids, and gels (using **P*n*** of Series B) were conducted on a Rigaku R-AXIS image plate system with Cu Kα X-rays (λ = 0.154 nm) generated by a Rigaku generator operating at 40 kV and 30 mA with the collimator at 0.5 mm (to obtain 0.5-mm-diameter beams). Data processing and analyses used *Materials Data JADE* (v 5.0.35) XRD pattern processing software. Samples were sealed in 0.5 mm glass capillaries (W. Müller, Schönwalde, Germany), and diffraction data were collected for 2 (neat powder) or 10 h (gel and liquid). The extended molecular lengths of the **P*n*** were calculated using *Materials Studio 4.3* software with the addition of the van der Waals radii[31] of terminal atoms. The energy minimization of gelator conformations was made using the Discover module.

UV–vis and CD. Spectra were recorded on a Chirascan circular dichroism spectrometer starting at 25 °C. A hot sol of **P7** was poured into a 1 mm path length quartz cell, which was sealed with a Teflon cap to avoid loss of liquid and cooled to room temperature to form a stable gel. The temperature-dependent spectra were recorded from low to high temperature in increments of 5 °C, allowing 10 min equilibration times after each increase, to a maximum of 55 °C. **P7** samples at very low concentrations (0.1%) were placed in thin path length cells (vide infra) for UV–vis and CD measurements. They were visually transparent.

Rheology. Measurements were performed using a stress-controlled rheometer (TA ARG2 instrument) equipped with stainless steel parallel plates (20 mm diameter, 1 mm gap). A liquid trap device was placed above the top plate to minimize evaporation. Before data were recorded, a hot aliquot of **P*n*** in 1-decanol was placed between the parallel plates of the rheometer and heated to 80 °C to ensure that a solution/sol was present. The sample was cooled to 20 °C at ~20 °C/min and incubated there for 15 min to reform the gel. Linear viscoelastic regions of the gel samples were determined by measuring the storage modulus, G' (associated with energy storage), and the loss modulus, G'' (associated with the loss of energy), as a function of the stress amplitude. Thereafter, the moduli were measured from 0.1 to 100 Hz at a constant shear stress in the linear region (12 Pa). The stress sweeps of each **P*n*** were measured 3 times and averaged using new samples for each run. Reported error limits are the difference between the value in one run and the average value. Also, recovery experiments at a constant frequency were performed by applying a constant oscillatory shear stress which was sufficient to destroy the gel structure (i.e., well beyond the linear viscoelastic region) for 2 min followed by a very small, constant oscillatory shear stress (1 Hz, 1 Pa) in the linear viscoelastic region while recording G' and G'' as a function of time.

RESULTS AND DISCUSSION

Purification and Purity of P*n*. The purification of **P*n*** was very difficult due to the presence of glucono groups. The initially purified material, referred to as Series A, was purified further to yield **P*n*** denoted as Series B. The melting points of the Series B **P*n*** are ~0.5 °C higher than those of Series A, and their melting ranges are somewhat narrower (Supporting Information Table S1). In addition, elemental analyses of Series B **P*n*** are closer to the values expected for a half-hydrate than those of Series A; although a common method to purify glucono-containing compounds is to wash the crude product with[32,33] or crystallize it from[34] methanol, **P4**–**P8** form very viscous suspensions in methanol without heating, or (as noted) gelate methanol with heating and cooling. Because the procedure for obtaining the Series B products is laborious and entails a significant loss of the product, and the difference between the elemental analyses for the two series is relatively small, < 2%,[35] we have used the series A material except where noted in the text; series B material was employed only where greater purity was deemed necessary.

Gelation Properties. The results from attempts to gelate 30 different liquids in the presence of 2.5% of the **P*n*** by heating and then cooling the mixtures, and the critical gelation concentrations (CGCs) of those that led to gels are summarized in Table 1. At this concentration, all of the **P*n*** dissolved in dimethyl sulfoxide (DMSO), *N*,*N*-dimethylformamide (DMF), pyridine, and *n*-butylamine without heating, and no gels were formed even when the solutions/sols were cooled to ~3 °C in a refrigerator for several hours. Also, the **P*n*** could not be dissolved in benzene, toluene, cyclohexane, *n*-nonane, diethyl ether, triethylamine, CH_2Cl_2, $CHCl_3$, and CCl_4 even when heated to the boiling points of these liquids. Both **P2** and **P3**[27] are ambidextrous—they can gelate both water and some organic liquids. **P4**, **P6**, **P7**, and **P8** were able to gelate the 10 alcohols tested (i.e., protic liquids), as well as acetonitrile, THF, acetone, ethyl acetate, and other relatively polar organic liquids, which are aprotic. However, they were unable to gelate water. The inability of the **P*n*** with longer linkers between the saccharide and pyrenyl groups to gelate water is most easily attributed to their greater hydrophobicity. The increasing number of methylene units also enhances the solubility of the **P*n*** in organic liquids, thereby altering the balance between aggregation and dissolution.[19] In addition, some gels marked with "b", such as **P4** in methanol, could be formed when their mixtures were sonicated at room temperature.[8] Gels such as **P3** in 1-decanol were thixotropic[36] at room temperature (i.e., these gels flowed immediately after being spun in a closed container on a spin coater for about 15 s and ceased to flow upon standing about 1 min without mechanical perturbation.

As mentioned, **P2** and **P3** gelate water, and so do the corresponding naphthyl analogues with short spacers, **N0** and **N2**. However, the comportment of the molecules with longer spacers are somewhat different: whereas **P4**–**P8** form homogeneous suspensions in water after the heating–cooling process, **N3**–**N6** dissolve in water only upon being heated and then precipitate when cooled to room temperature.[19] More importantly, the **P*n*** can gelate not only the protic liquids gelated by **N*n***, but also a wider variety of aprotic liquids. From a structural standpoint, the origin of the improved gelating ability of the **P*n*** series may be related to their increased solubility in organic liquids and their enhanced π–π stacking.[37] Both factors are known to be important contributors to the ability of many other molecules to be effective LMOGs.[4,14] However, molecular packing considerations, to be discussed below, may play an important role as well.

Because gels of **P2** became precipitates after one day, their CGCs could not be determined with confidence and they are not reported. Of the gels present at 2.5% of **P*n***, all except **P2** were stable in sealed vessels at room temperature for at least one month. The T_{gel} values of gels of 2.5% **P*n*** in the same liquid are near each other as a result of the similar structures and CGCs of the **P*n***. In some cases at 2.5%, such as **P3** in 1-decanol and **P7** in acetone, the T_{gel} values are much higher than those of other **P*n*** gels; this result follows from **P3** and **P7** exhibiting the lowest CGCs in these liquids. The data in Figure S1 show that the T_{gel} of gels of **P7** increase with increasing concentration up to ~1.5% and then reach a "plateau" value.

Many of the CGCs are less than 1%, so that the **P*n*** are "supergelators".[38] In fact, the CGCs of **P3** in 1-butanol, 1-

dx.doi.org/10.1021/la304957n | *Langmuir* 2013, 29, 793–805

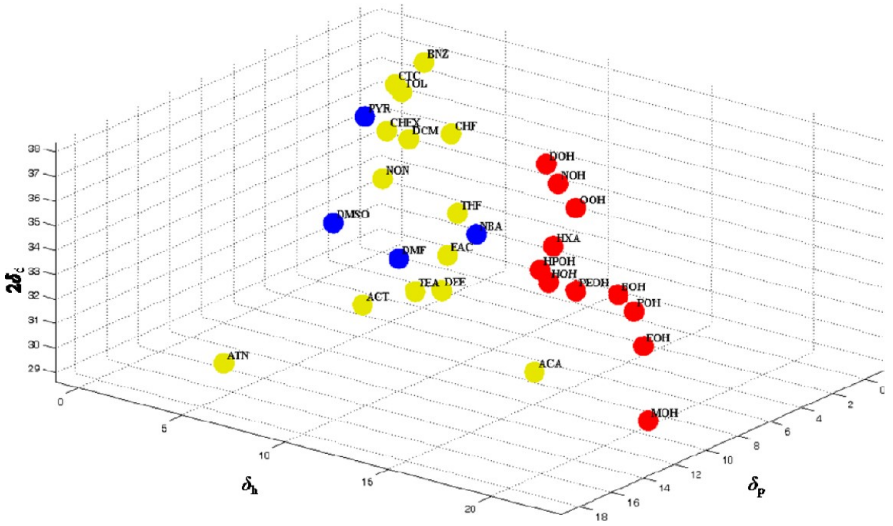

Figure 1. Solubility data for 2.5% **P3** in neat liquids represented in Hansen space. Blue (soluble), red (gel), and yellow (insoluble).

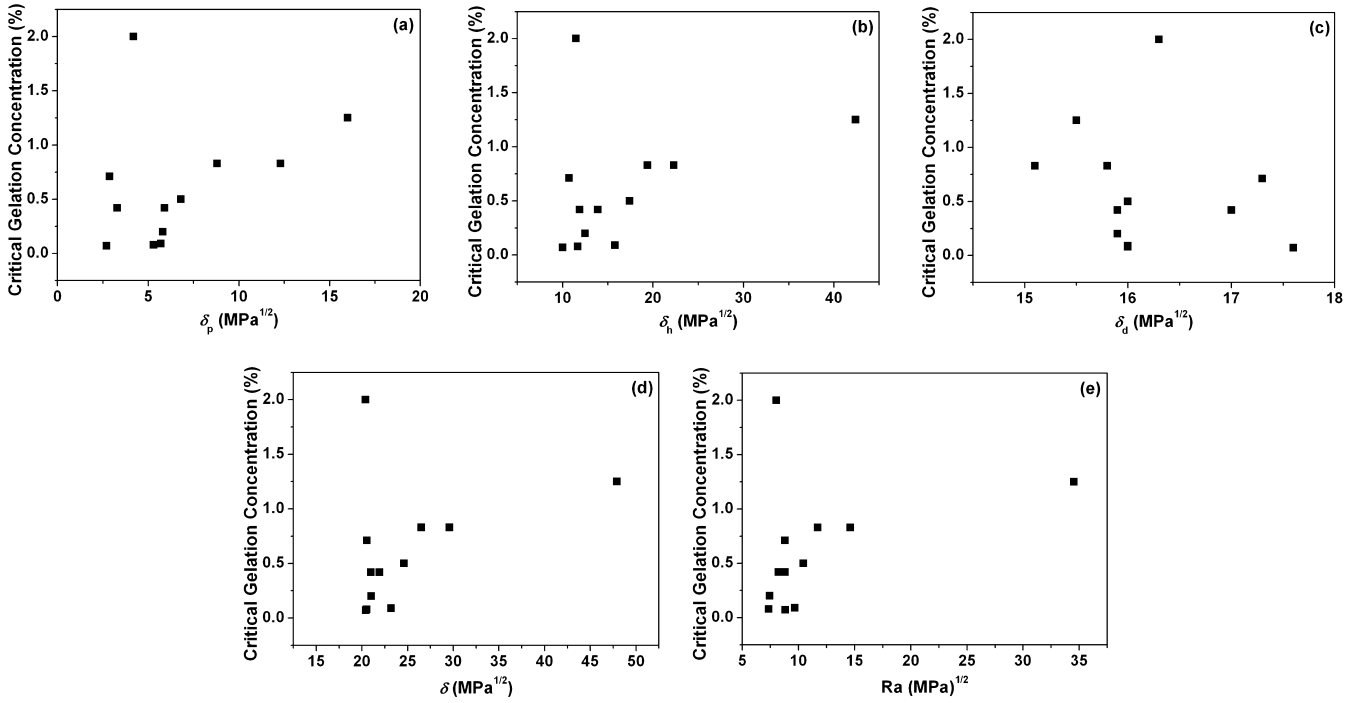

Figure 2. Critical gelation concentrations (CGCs) of **P3** in some liquids as a function of (a) δ_p, (b) δ_h, (c) δ_d, (d) overall Hansen solubility parameter (δ), and (e) R_a in Hansen space from **P3**.

heptanol, and 1-decanol, **P6** in acetonitrile, **P7** in acetonitrile and ethyl acetate, and **P8** in ethyl acetate are less than 0.1%! These concentrations translate to an ability of one molecule of **P3** to immobilize ~3850 molecules of 1-decanol, and one molecule of **P7** to immobilize ~7300 molecules of ethyl acetate. By contrast, the CGC of only **N6** in acetonitrile is <0.1%.[19] By this criterion, the **P*n*** are again more efficient gelators than their **N*n*** analogues.

Gelation and Hansen Solubility Parameters (HSPs). In an attempt to understand better the relationship between the gelator structures and the range of liquids that they are (and are not!) able to gelate, we have employed an analysis using HSPs. Table S2 summarized the HSPs of the liquids.[23] The Hansen spaces[25] are shown in Figure 1 for **P3** and in Figures S2−S6 for the other **P*n***. As a result of the extremely high δ_h value of water and the obvious inability of current Hansen theory to provide reasonable results for the **Pn** samples in water—they skewed the plots—data from these samples were not included in the analyses. The polar interaction parameter, δ_p, and hydrogen bonding interaction parameter, δ_h, of the 30 liquids examined here cover a large portion of Hansen space, while the dispersive interaction parameter, δ_d, falls within a narrow range ($14.5 < \delta_d < 19$ MPa$^{0.5}$). In all of the graphs, the point for water is an outlier; current theory does not take into full account the properties of some of the liquids, at least as they apply to gelation by LMOGs. Furthermore, δ_h for the gelated liquids of **P2** (Figure S2) and **P3** (Figure 1) span a larger range of values (from 10 to 42 MPa$^{0.5}$) than those of **P4**−**P8** (from 6.1 to 22.3 MPa$^{0.5}$). The ranges are consistent with **P2** and **P3** being ambidextrous and **P4**−**P8** being only gelators of organic

dx.doi.org/10.1021/la304957n | *Langmuir* 2013, 29, 793−805

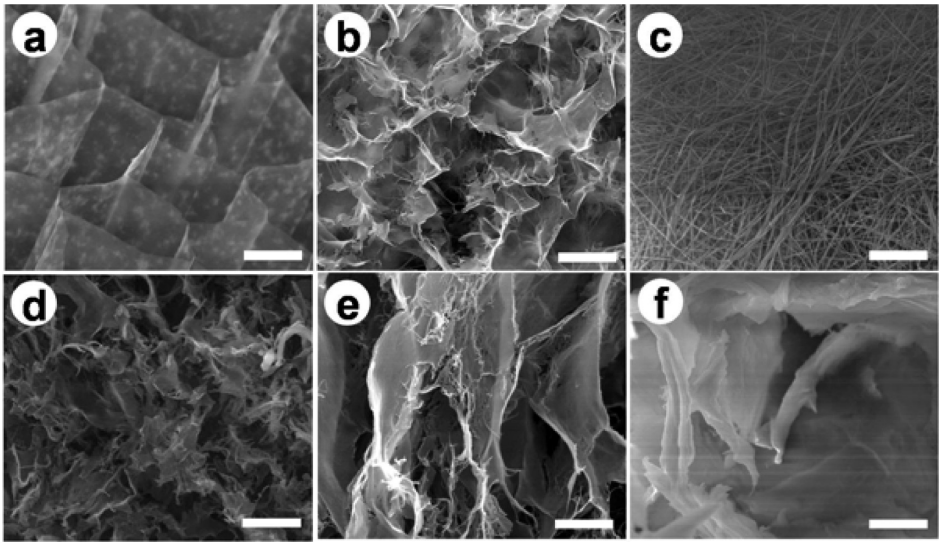

Figure 3. SEM images of xerogels prepared from 2.0% **P*n***: (a) **P2** in water, (b) **P3** in water, (c) **P4** in acetonitrile, (d) **P6** in acetonitrile, (e) **P7** in acetonitrile, and (f) **P8** in acetonitrile. Bar distances = 10 μm.

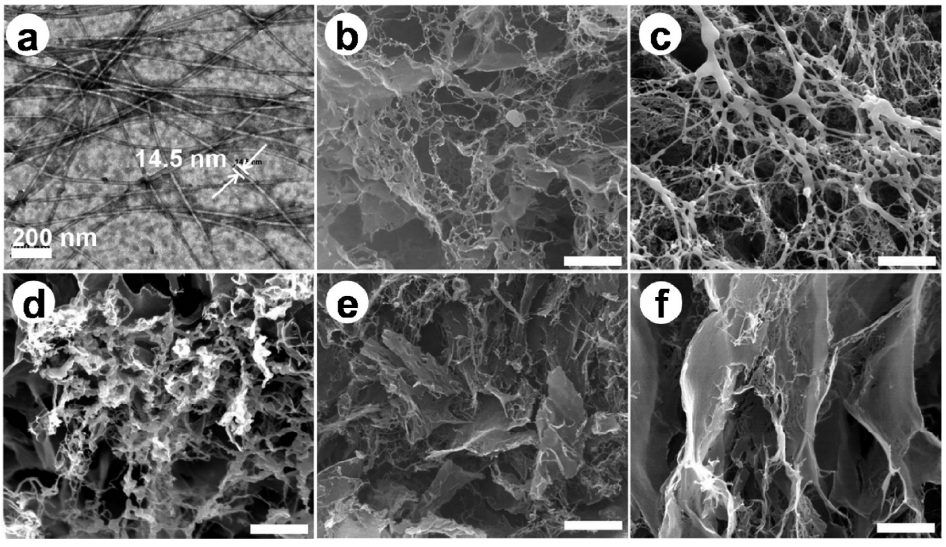

Figure 4. (a) TEM image of a dried sol of 0.05% **P7** in acetonitrile. SEM images of xerogels made from **P7**/acetonitrile gels at initial [**P7**] = (b) 0.2%, (c) 0.5%, (d) 1.0%, (e) 1.5%, and (f) 2.0%. (Distance bars = 10 μm except in (a)).

liquids.[25,26] In addition, the Hansen spaces of **P4**−**P8** are almost the same as a consequence of their similar gelation behavior in the liquids. However, the difference between Hansen spaces of **P3** and **N3** is obvious: there are more gel points in the Hansen space of **P3** but more soluble points in that of **N3** (Figure S7). For example, whereas **P3** is an ambidextrous gelator, **N3** is only an organo-gelator, and methanol is gelated by **P3** while **N3** dissolves in it.

Figure 2 shows correlations of the individual HSPs, the overall HSPs, and the distances in Hansen space from **P3** with its CGCs in the gelated liquids. Although δ_d (Figure 2c) does not appear to have a clear effect on the gelating ability of **P3**, the CGCs increase roughly with increasing δ_p, δ_h, overall δ and R_a (Figure 2a,b,d,e, respectively); the gelating ability of **P3** decreases in liquids with higher polarity and more hydrogen-bonding interactions.[26] Similar correlations are found for the other **P*n*** (Figures S8−S11). However, there is no trend that we can discern between the Hansen parameters and the CGCs of the **P*n*** as a function of the linker length, *n*. Regardless, it is clear that the changes in the gelating abilities of the LMOG homologues are a result of primarily polar and H-bonding interactions between the gelator molecules and the liquid components.

Morphology Studies. SEM images of the immobilizing networks of xerogels from gels with one liquid and different **P*n*** homologues were compared (Figure 3). The xerogel samples were homogeneous, and SEM images taken at different parts of each sample were like the ones shown. The results demonstrate, as expected, that the morphologies of the xerogels depend upon both the structures of the gelator and the nature of the liquid. The aggregates of **P2** from its hydrogel appear like a beehive, and differ from those of **P3**. The SEM images of the xerogels from gels of **P4**−**P8** in acetonitrile were also compared. The xerogel from **P4** in acetonitrile has a fibrous network structure, while those of **P6**, **P7**, and **P8** in acetonitrile, although similar to each other, display belt-like structures. If the xerogel networks are like those in the actual gels (and this is not

dx.doi.org/10.1021/la304957n | *Langmuir* 2013, 29, 793−805

always the case[22,39]), the images suggest that aggregation increases with increasing spacer length *n*.

In an attempt to reveal the nature of the aggregates in greater detail, both TEM and SEM images were recorded for samples starting from sols and xerogels of **P7** in acetonitrile. Careful inspection of TEM images of fibrils made from a 0.02% sol of **P7** (Figure S12) appear to contain left-handed twisted fibers with ca. 4.5 nm width. Increasing the concentration of **P7** to 0.05% resulted in a large amount of thread-like fibers with an average diameter of 14.5 nm (Figure 4a) and without apparent twisting (although some are bent). At still higher concentrations (Figure 4b–f), the fibrils become thicker and integrate into networks (Figure 4b), and finally fuse into lamellar-like structures (Figure 4f).

The static contact angle of a water droplet on a film of the xerogel made from 1.5% **P7** in acetonitrile, 116.5 ± 3.0° (Figure S13), was larger than that on a film of the xerogel from 1.5% **N2** in acetonitrile, 105.1 ± 1.0°.[19] The more hydrophobic surface of the xerogel from **P7** is consistent with the aforementioned larger aromatic surface areas of pyrenyl than naphthyl and the longer spacer length.

Packing Arrangements from XRD Studies. Many diffraction peaks are detectable in the XRD diffractograms of neat **P*n***, especially **P2** and **P3** (Figure S14). The similarity among the diffractograms of **P4**–**P8** is indicative of their packing arrangements being similar as well; all can be indexed to monoclinic lattices. In addition, the small incremental increases in the *d* spacings calculated from the lowest angle peaks in the diffractograms and the similarity between the absolute *d* values and the lengths calculated for the extended conformations of interdigitated pairs of **P4**–**P8** molecules (e.g., for **P7**, the *d* value is 4.16 nm and the calculated end-to-end distance of an interdigitated dimer is 4.36 nm) provide additional support for their packing arrangements being closely related. However, the morphologies of **P2** and **P3** are different from each other and from those of **P4**–**P8** (Table S3). The *d* value of the lowest angle peak of **P2** is almost equal to the calculated length of an extended **P2** molecule, and that of **P3** is longer than the calculated length of an extended **P3** molecule, but shorter than the calculated length of an interdigatated pair (Figure S15).

The XRD patterns of neat **P7**, a xerogel from a **P7**–acetonitrile gel, and a gel of **P7** in acetonitrile are compared in Figure S16. The diffraction peaks of the **P7** component in the gel were identified by subtracting empirically the amorphous scattering of the acetonitrile liquid from the total gel diffractogram.[40] Unlike the monoclinic lattice of neat **P7**, the three reflection peaks of the **P7** xerogel correspond to *d* values of 4.16, 2.05, and 1.39 nm and follow a 1:(1/2):(1/3) progression ratio consistent with (but not definitive for, given the dearth of peaks) a lamellar organization.[41] A lamellar packing arrangement is suggested as well by the TEM (Figures 4a and S12) and SEM (Figure 4b–f) images of fibers in the xerogel. However, the diffraction pattern of the **P7** gel is less clear; it consists of one small peak with a *d* value of 4.16 nm and another broad peak at higher angle (smaller distance). The differences between the XRD patterns and electron microscopy images of neat **P7** and its xerogel demonstrate that the molecular packing arrangements of **P7** in the two phases are not the same, and that **P7** molecules in the xerogel adopt the more regular packing arrangement. Although the basis for the differences cannot be discerned from the information in hand, the three phases of **P7** display the same lowest angle *d* value, 4.16 nm. That distance is suggestive of lamellar arrangements for all and is close to the diameter of the smallest fibrils observed by TEM (Figure S12). Thus, we hypothesize that the packing arrangement of the **P7** molecules in the strands, fibers, and sheets, of the xerogels involves an interdigitated head-to-tail orientation (Scheme S2).

Spectroscopic Studies. With increasing temperature, the peaks in the UV–vis absorption spectra of 0.1% **P7** in acetonitrile at ~280, 350, and 380 nm increase and that at ~295 nm decreases (Figure 5). Such changes are expected if

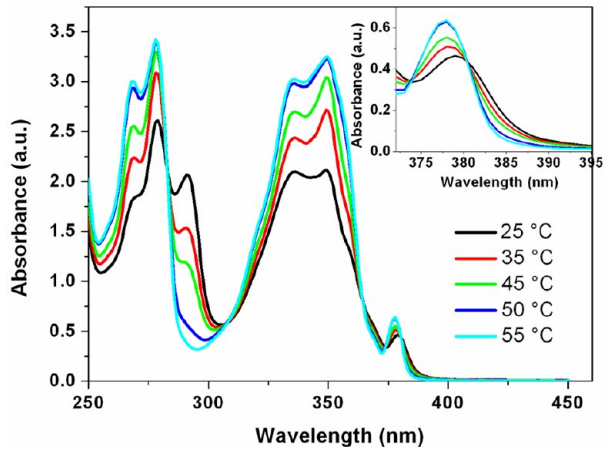

Figure 5. Temperature dependence of UV–vis spectra of 0.1% **P7** in acetonitrile. Inset: magnified 372–395 nm spectral region.

π–π stacking of pyrenyl moieties plays an important role in the gelation.[42] Because the absorption band at 377 nm is red-shifted by about 3 nm as the sol cools to its gel state (where intermolecular association among **P7** molecules increases), the pyrenyl groups appear to be in J-type aggregates (as do the **N2** molecules in acetonitrile[19]).[42] Also, the presence of 5 isosbestic points indicates that the species in the sol and gel phases interconvert directly, without the presence of a significant amount of any new intermediates. We propose that an important driving force for J-type aggregation of the pyrenyl groups is related to H-bonding of the glucono units at the opposite end of the **P7** molecules.

Circular dichroism (CD) spectra of **P7** in its sol and gel phases (Figure 6) show a clear increase in intensity with increasing aggregation. The CD intensity frequently increases when chiral LMOG molecules self-assemble with appropriate orientations.[13,43] The influence of increased aggregation on CD intensities is most apparent in Figure 6b where the very strong bands from 0.1% **P7** in acetonitrile at 25 °C virtually disappear at 55 °C; as indicated in Figure S17, the intensity changes are completely reversible with temperature. Thus, the CD signals originate from the chirality of the supramolecular aggregates rather than from the inherent chirality of the LMOG molecules.[44] Analogous results were obtained from **N2** in acetonitrile.[19] Taken together, these results support a model in which the **P7** molecules are organized in helical arrangements within their fibrillar networks.[45]

Fluorescence measurements have been used as well to probe the self-assembly of 1.5% **P7** (Series B) in acetonitrile (Figure 7). Emissions from both phases include structured peaks from monomeric pyrenyl singlet states and a broad band from an excimeric emission (Figure 7a). Although the absorption and CD spectral studies show that the **P7** molecules are more

dx.doi.org/10.1021/la304957n | *Langmuir* 2013, 29, 793–805

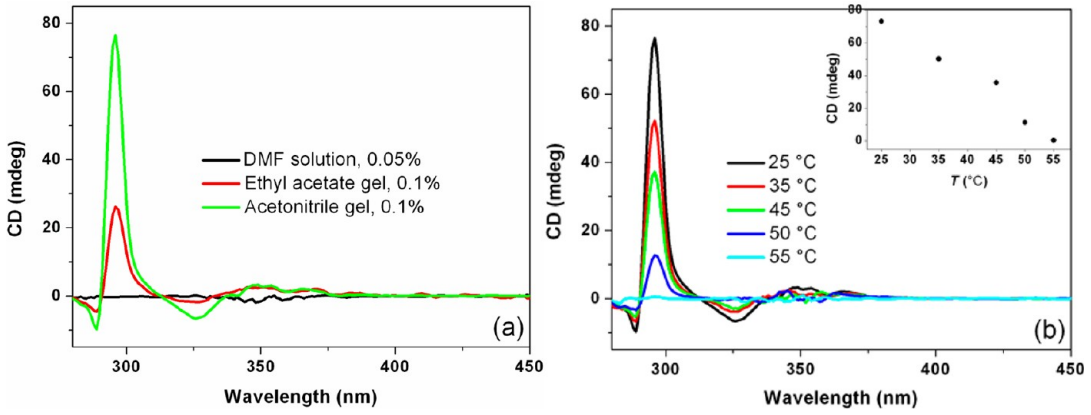

Figure 6. (a) CD spectra of **P7** at 0.05% in its DMF sol, and in its transparent gels at 0.1% in ethyl acetate and acetonitrile at 25 °C. (b) Temperature-dependence of the CD spectrum of a transparent gel of 0.1% **P7** in acetonitrile. Inset: CD intensity at 295 nm as a function of temperature. The optical densities of these samples were less than 0.7 at the wavelength maxima near 300 nm.

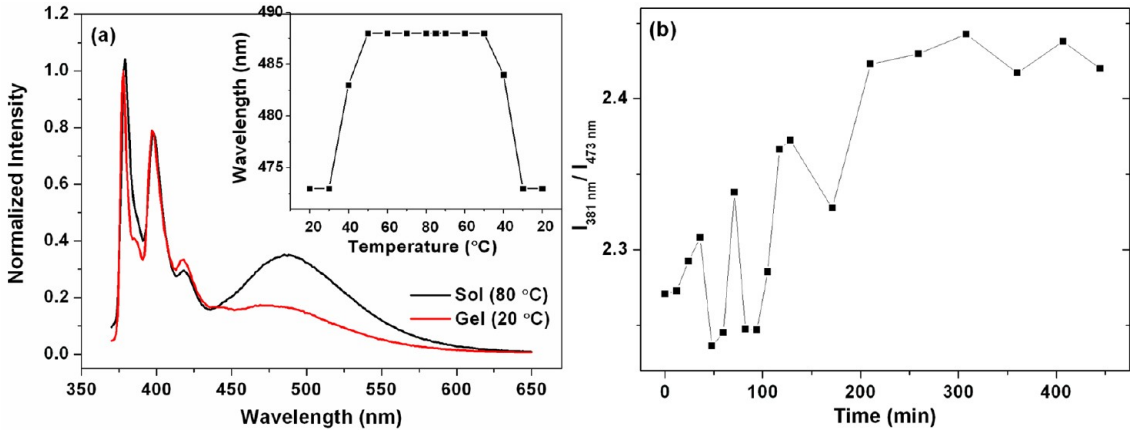

Figure 7. (a) Fluorescence spectra (λ_{ex} 350 nm; normalized at 378 nm) of 1.5% (2.6×10^{-2} M) **P7** (Series B) in acetonitrile in the gel (20 °C) and sol (80 °C; T_{gel} = 79 °C) phases. The inset shows the temperature-dependent wavelength maximum of excimeric emission. (b) Effect of time on the value of the $I_{381\ nm}/I_{484\ nm}$ emission ratio after formation of the gel by cooling its sol rapidly to 20 °C.

associated in the gel phase than in the sol phase, the relative intensity at the wavelength maximum of the excimeric emission is higher in the less aggregated sol phase. The same trend was found in the **N2** system,[19] but some others are known to behave differently.[22] However, deconvoluting the spectra into their monomeric and excimeric components was not possible due to the multiple species present (as indicated by the excitation spectra in Figure S18). Regardless, the spectra in Figure 7a show a clear and marked difference between the positions and shapes of the excimeric components of emission in the gel and sol phases. As indicated by the inset of Figure 7a, the changes are reversible. Although the relative intensities of the monomer and excimer emissions in the sample cooled to room temperature from the sol phase change with time (increasing $I_{381\ nm}/I_{473\ nm}$ intensity ratio; Figure 7b), the shape and emission maximum of the excimer band change only slightly (Figure S19). Thus, over time, the **P7** molecules within the initially formed gel network rearrange to environments less conducive to excimer formation. The change of the ratio with time may be due to Ostwald ripening[46] and related phenomena. Similar phenomena have been reported by others in different gelator assemblies.[47,48]

Note also that the maximum emission wavelength of the excimeric emission of the sol phase, 488 nm, is red-shifted by 10 nm with respect to that of the gel phase,[49] and the red shift occurred with increasing temperature (inset of Figure 7a). This difference may arise from a change in the local polarity experienced by the pyrenyl units in the two phases or by an inability of the excimeric geometries to be achieved rapidly (leading to blue-shifted emissions). At the elevated temperatures of the melted gel (i.e., the sol phase), pyrenyl units are more exposed to acetonitrile molecules which provide a relatively polar microenvironment. In the gel phase, the polarity of the microenvironment of pyrenyl units may be lower due to $\pi-\pi$ stacking of pyrenyl units and exclusion of acetonitrile molecules from their immediate vicinity. In such a case, the emission wavelength maximum of the excimer would be blue-shifted in the gel phase with respect to the sol phase.[50] A lower average polarity for the pyrenyl groups of **P7** in the gel phase is indicated also by a decrease in I_1/I_3, the ratio between the intensities of the first and third monomer vibronic peaks, from 1.31 in the sol phase to 1.24 in the gel phase (the I_1/I_3 ratio of pyrene in acetonitrile is 1.79, and in less polar ethanol and benzene is 1.18 and 1.05, respectively).[51]

Overall, these results indicate that the greater mobility of the **P7** molecules in the sol phase allows facile reorientations within the excited singlet lifetimes of neighboring pyrenyl groups into the necessary excimeric geometry, and that the preferred orientations of neighboring pyrenyl groups in the networks of the gel phase are not very close to the optimal excimeric

dx.doi.org/10.1021/la304957n | *Langmuir* 2013, 29, 793−805

geometry and are less able to form excimers due to more severe packing constraints.

As mentioned previously,[19] glucono units have been introduced into the **P*n*** structures as a means to promote strong intermolecular H-bonding interactions and to enforce segregation among the structural units of the **P*n*** as they aggregate. The spectroscopic tools employed in the discussion above probe primarily the pyrenyl part of the **P*n*** molecules. FTIR spectra of the xerogels of **P7** from acetonitrile and ethanol, and of **P7** in a DMF solution/sol have been used to investigate the expected H-bonding interactions of the glucono part (Figure S21). The spectrum of **P7** in DMF contains bands at 3326, 1639, 1313 (1140), and 1540 cm^{-1} that can be attributed to the stretching vibrations of OH(NH), CO, and SO, and the bending vibration of NH, respectively.[52] In the xerogels, these bands shift to 3274, 1624, 1304 (1128), and 1545 cm^{-1} (**P7**/ethanol) and to 3278, 1625, 1307 (1132), and 1548 cm^{-1} (**P7**/acetonitrile). These shifts are consistent with the formation of *inter*molecular H-bonds as aggregation of **P7** occurs.[16]

Additional information about the nature of the aggregation process for **P7** was obtained from the temperature and concentration dependence of its ^{1}H NMR spectra in DMSO-d_6, a liquid in which the gelator is readily soluble (Figure S22). At 4.0% (0.07 mol/L) **P7**, the proton signals at room temperature can be assigned based on molecules with similar structures.[53] Hydroxyl peaks from the glucono moiety shifted from 5.35 and 4.58−4.39 at 25 °C to 4.98 and 4.18−4.10 ppm at 85 °C. The NH signals shifted from 8.09 and 7.46 to 7.68 and 7.20 ppm over the same temperature range (Figure S22a). The observed shifts are attributed to decreased *inter*- and/or *intra*-molecular hydrogen-bonding interactions as the temperature is increased.[54] To distinguish between the *inter*- and *intra*-molecular interactions, spectra at 25 °C were recorded at different concentrations (Figure S22b); as the concentration of the gelator increases, the relative contribution of intermolecular H-bonding interactions also increases. In the range of 1.0% (0.02 mol/L) to 8.0% (0.14 mol/L) **P7**, signals of the hydroxyl and NH groups shifted slightly to lower field with increasing concentration. Given the large temperature dependence of the hydroxyl proton signals at 4.0% (0.07 mol/L) **P7** and the much smaller dependence as the concentration was doubled to 8% (0.14 mol/L), we conclude that the perturbations caused by *inter*-molecular interactions are relatively small. The *intra*-molecular H-bonding networks are largely retained as aggregation occurs and the influence of the glucono−glucono interactions on the nature of the aggregate structures is primarily from electrostatic forces (i.e., polarity). Of course, the balance between *inter*- and *intra*-molecular H-bonding interactions within aggregates of the **P*n*** will change with the characteristics of the liquid employed. However, the results in DMSO seem to point to the greater importance of effects more easily explained by Hansen-type parameters.

In Hansen space of **P7** (Figure S23), DMSO is outside the soluble sphere but inside the gel shell (at 2.5% concentration), and the distance (R_{DMSO}) from **P7** (δ_p = 10.08 $MPa^{0.5}$, δ_h = 9.58 $MPa^{0.5}$, and δ_d = 17.10 $MPa^{0.5}$) to DMSO is 6.87 $MPa^{0.5}$ (eq 2); this distance is between R_{sol} (5.53 $MPa^{0.5}$, the radius of the soluble sphere) and R_{gel} (8.79 $MPa^{0.5}$, the radius of the gelation sphere). In general, if this distance is smaller than an empirical and case-specific value of R_{sol}, the molecule and the liquid are expected to have a high probability of being miscible.[25,55] Thus, **P7** molecules may be somewhat aggregated in DMSO—R_{DMSO} is less than R_{gel}—consistent with the proton shifts when changing the concentration of **P7** in DMSO. However, because δ_h (10.2 $MPa^{0.5}$) and δ_d (18.4 $MPa^{0.5}$) of DMSO are very close to those of **P7**, much of the **P7** may remain dissociated even at the highest concentration investigated, 8%.[55] The relatively small dependence of the hydroxyl proton signals on concentration may be a consequence of the ease of *intra*molecular H-bonding that competes with *inter*molecular H-bonding even when significant aggregation of the **P7** molecules occurs. Such a scenario also explains the small variations in chemical shifts of the NMR spectra when temperature or concentration is changed.

The pyrenyl signals provide additional information about $\pi-\pi$ stacking.[16] The chemical shift of the α-H ("H_h" in the inset of Figure S22a) of the pyrenyl ring at 4% **P7** is at 9.00−9.03 ppm at 25 °C and moves to 9.03−9.07 ppm at 85 °C (Figure S22a); the same signal is shifted slightly to lower field with increasing concentration (Figure S22b). These modest shifts are consistent with the UV−vis and fluorescence results which indicate that the pyrenyl units are not oriented well with respect to each other even in the gel phase. However, the change in the chemical shift of the α-H (next to the sulphonyl group) in the naphthyl ring of **N2** in DMSO-d_6[19] is smaller than that of H_h in the pyrenyl analogues. This observation is suggestive of but not definitive proof of better $\pi-\pi$ stacking in the gel networks of the **P*n*** series.

Rheology of the Gels. A strict definition of a gel must include specific mechanical behavior. For that reason and because some of the gels in Table 1 are thixotropic at room temperature, the rheological properties of several of the **P*n*** gels have been examined.

2.0% **P3**-**P8**/1-decanol gels were selected for investigation of the effect of spacer length on the mechanical properties of the gels. The rheology of the **P2** gel was not examined due to its instability; as mentioned, it undergoes phase separation at room temperature after ∼1 day. The storage modulus, G', and loss modulus, G'', were measured as a function of shear stress at 20 °C. The shear stress sweeps of each **P*n*** in Figure 8 are the average of 3 measurements, and the G' and G'' values at stress = 10 Pa, G'/G'' ratios, and yield stress are summarized in Table S4. From the results in Figure 8, the initial G' is higher than G'' by about 1 order of magnitude in each sample and remains

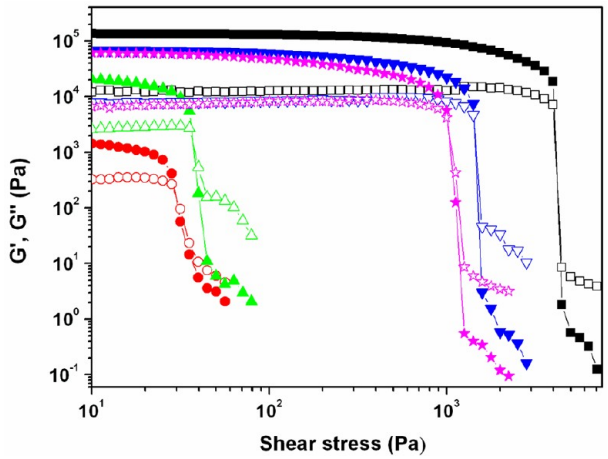

Figure 8. Log−log shear stress sweeps (frequency = 1.0 Hz) for gels of 2.0% (■) **P3**, (red ●) **P4**, (green ▲) **P6**, (blue ▼) **P7**, and (pink ★) **P8** in 1-decanol at 20 °C. G', closed symbols; and G'', open symbols.

dx.doi.org/10.1021/la304957n | *Langmuir* 2013, 29, 793−805

higher over large ranges of shear stress. This is the comportment expected of a true gel phase.[56] With a gradual increase in applied stress, both G' and G'' remain almost invariant (i.e., in the linear viscoelastic region), and at a certain yield stress, they cross, indicating a mechanical breakup of the gels; beyond the yield stress, they deviate from linearity. From the results in Figure 9, both the value of G'/G'' at the initial

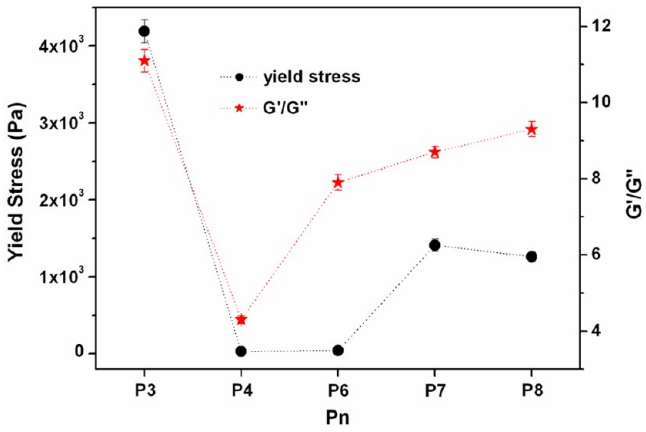

Figure 9. Yield stress and G'/G'' ratios of gels of 2% **P3**–**P8** in 1-decanol at 20 °C.

stress and yield stress decrease and then increase with increasing length of the spacer of **P*n***. Furthermore, the **P4** gel is the most fragile as indicated by its lowest G'/G'' value (4.3 ± 0.1) and yield stress (30 ± 3 Pa). The **P3** gel is the most stable mechanically; it possesses the largest G'/G'' ratio (11.1 ± 0.3) and yield stress (4460 ± 160 Pa). Because the CGCs of **P3**–**P8** in 1-decanol are very low (<0.3%) and the concentrations employed in the rheological studies are 2.0%, the large differences in the mechanical properties of the **P*n*** gels cannot be attributed to the small concentrations of the gelator molecules not incorporated within the networks. The G'/G'' values at the initial stress and the yield stresses (except **P3**) indicate that the mechanical properties of the gels improve with increasing spacer length of the **P*n*** (Figure 9).[57]

X-ray diffractograms of even 10% **P*n*** in 1-decanol (Figure S24 and Table S5) provide very little useful information about the molecular packing arrangements in these gel networks; they lack sharp diffraction peaks. The similar optical microscopy images of 2% **P3**–**P8** in 1-decanol (Figure S25) cannot supply any information about the different mechanical stabilities of these gels, either. However, because the T_{gel} and G'/G'' values of 2% **Pn** in 1-decanol (Figure S26) follow similar trends, the mechanical strengths may be related to the energy needed to melt the networks.

P7 was chosen to investigate the role of gelator concentration on the rheological properties of the gels. As the **P7** concentration in 1-decanol was increased from 0.5% to 2.0% (Table S6), G'/G'' at stress = 10 Pa increased drastically, from 0.9 ± 0.05 to 8.7 ± 0.15, and the yield stress changed from a very low value, 7.9 ± 1 Pa, to 1412 ± 80 Pa. Thus, both the elastic property (including thixotropy) of the gel and the stability of the gel network depend acutely on gelator concentration.[57] Also, as expected of a true gel,[56] G' of a 2% **P7** in 1-decanol is nearly constant over a frequency range of 0.01 to 100 Hz and remains greater than the associated G'' (Figure S27). This is the typical behavior of a gel (albeit a weak one, given the absolute magnitude of G').

Finally, as mentioned above, some of the gels in Table 1, including 2% **P7** in 1-decanol, show thixotropic properties at room temperature. In order to determine the magnitude and reproducibility of the thixotropic behavior, the shear–stress stimulus response was examined. A 2% **P7** in 1-decanol gel was sheared at a constant stress of 1680 Pa for 2 min, and then the evolution of the moduli as functions of time was monitored. During the recovery process, a shear stress of 1 Pa and a frequency of 1 Hz were applied to minimize perturbations to the gel reformation; the time axis was started as rapidly as the rheometer allowed (ca. 2 s delay) after the end of the destructive shear (Figure S28). The inset reveals that the gel network was destroyed partially by the high stress; it became more viscous than elastic as evidenced by $G' < G''$. However, the sample recovered 55% of its elastic properties after cessation of the high stress.[57,58]

Model for Molecular Packing of P*n* Molecules in their Gel Networks. On the basis of the data presented above, a

Chart 2. Schematic Representation of a Possible Aggregation Mechanism for P7 in Acetonitrile

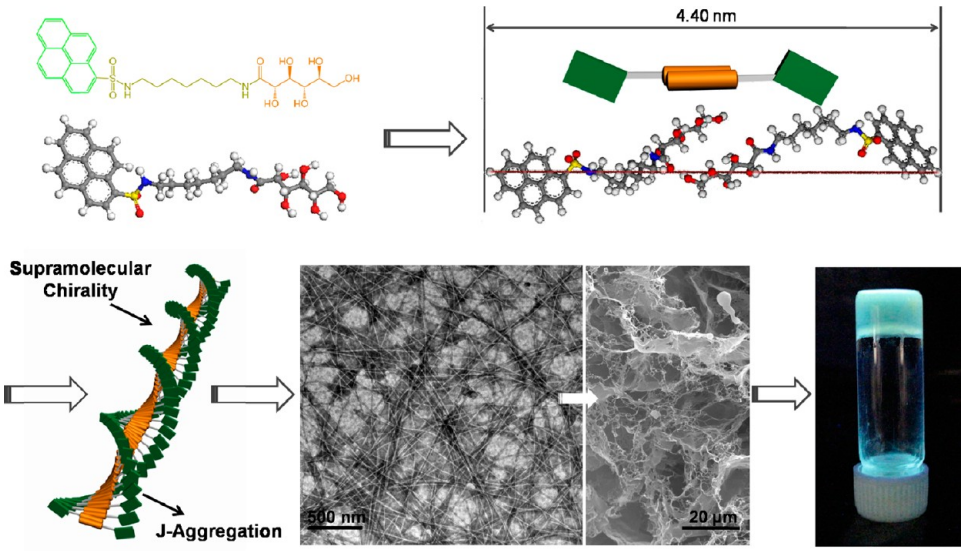

dx.doi.org/10.1021/la304957n | Langmuir 2013, 29, 793–805

possible formation process for the gel networks of **P7** in acetonitrile (and, presumably, the other **P*n*** to varying degrees) is proposed (Chart 2). It relies on the conclusions derived from several experimental observations:

1. Spectroscopic measurements indicate that $\pi-\pi$ stacking of J-type aggregates and intermolecular H-bonding are important driving forces for the formation and maintenance of the gel networks. Synergistic operation of the forces enhances the probability that the gelator molecules will aggregate into fibrils whose diameter is equal to the length of an interdigitated pair of **P7** molecules.
2. From contact angle measurements, the surfaces of the fibrils from the organogels are hydrophobic.
3. CD and TEM measurements indicate that the individual fibrils aggregate into twisted, thin fibers which subsequently aggregate into belts and then fuse into the lamellar structures implied by the XRD data.

CONCLUSIONS

In summary, a series of fluorescent **P*n*** LMOGs, based on glucono and pyrenyl groups, has been synthesized and their abilities to gelate a wide variety of liquids have been examined empirically and by Hansen solubility parameters. The nature of the gels and their properties, determined by a variety of techniques, have allowed several conclusions about the importance of spacer lengths between the glucono and pyrenyl groups from internal comparisons of the **P*n*** and external comparisons between the **P*n*** and naphthyl analogues, **N*n***, to be derived. The range of gelator behaviors among the **P*n*** is extremely broad: some of the **P*n*** are ambidextrous, some are "supergelators", and some of their gels are thixotropic. As expected, $\pi-\pi$ stacking (in J-type aggregates) and intermolecular H-bonding interactions synergistically drive the formation of the gel networks. This series of LMOGs demonstrates how the addition or removal of even one methylene group in a fairly large molecule can alter dramatically its ability to self-assemble and to interact with a liquid.

The correlations between the gelation behaviors of the **P*n*** and Hansen solubility parameters indicate that the changes among the LMOG homologues are primarily a result of polar and H-bonding interactions between the gelator molecules and the liquid components. Also, the morphologies and microstructures of the gel networks depend strongly upon the length of the spacer group in the **P*n***. Finally, the mechanical properties of the gels can be controlled to some extent by adjusting the spacer length or by changing the gelator concentration.

The results derived from these studies offer insights into how to design other surfactant-containing LMOGs. We intend to explore the extent to which the design criteria implied by the results with the **P*n*** (as well as the comparisons made with the structurally similar **N*n***) can be used to construct new classes of molecules with predefined gelating properties.

ASSOCIATED CONTENT

Supporting Information

Synthesis and characterization of **P*n***, Hansen spaces of **P*n*** in 30 liquids, the correlation of Hansen solubility parameter and CGCs, contact angle figures of the xerogel from **P7** in acetonitrile, X-ray diffraction patterns, rheological data, and additional spectra and images. This material is available free of charge via the Internet at http://pubs.acs.org.

AUTHOR INFORMATION

Corresponding Author

*E-mail: yfang@snnu.edu.cn (Y.F.), weissr@georgetown.edu (R.G.W.).

Notes

The authors declare no competing financial interest.

ACKNOWLEDGMENTS

We thank the US National Science Foundation and the Natural Science Foundation of China (20902055, 20927001, 91027017, and 21273141) and the 13115 Project of Shaanxi Province (2010ZDKG-89) for their financial support. This work was also supported by "Program for Changjiang Scholars and Innovative Research Team in University" of China (IRT1070). We are also extremely grateful to Prof. Laurent Bouteiller for useful discussions concerning Hansen plots as applied to gels.

REFERENCES

(1) Vemula, P. K.; Li, J.; John, G. Enzyme catalysis: tool to make and break amygdalin hydrogelators from renewable resources: a delivery model for hydrophobic drugs. *J. Am. Chem. Soc.* **2006**, *128*, 8932−8938.

(2) Zhang, M. M.; Sun, S. T.; Yu, X. D.; Cao, X. H.; Zou, Y.; Yi, T. Formation of a large-scale ordered honeycomb pattern by an organogelator via a self-assembly process. *Chem. Commun.* **2010**, *46*, 3553−3555.

(3) Adhikari, B.; Banerjee, A. Short-peptide-based hydrogel: A template for the in situ synthesis of fluorescent silver nanoclusters by using sunlight. *Chem.—Eur. J.* **2010**, *16*, 13698−13705.

(4) Terech, P.; Weiss, R. G. Low molecular mass gelators of organic liquids and the properties of their gels. *Chem. Rev.* **1997**, *97*, 3133−3159.

(5) Sangeetha, N. M.; Maitra, U. Supramolecular gels: functions and uses. *Chem. Soc. Rev.* **2005**, *34*, 821−836.

(6) Esch, J. H. v.; Feringa, B. L. New functional materials based on self-assembling organogels: from serendipity towards design. *Angew. Chem., Int. Ed.* **2000**, *39*, 2263−2266.

(7) Murata, K.; Aoki, M.; Nishi, T.; Ikeda, A.; Shinkai, S. New cholesterol-based gelators with light- and metal-responsive functions. *J. Chem. Soc. Chem. Commun.* **1991**, 1715−1718.

(8) Naota, T.; Koori, H. Molecules that assemble by sound: an application to the instant gelation of stable organic fluids. *J. Am. Chem. Soc.* **2005**, *127*, 9324−9325.

(9) Liu, J.; He, P. L.; Yan, J. L.; Fang, X. H.; Peng, J. X.; Liu, K. Q.; Fang, Y. An organometallic super-gelator with multiple-stimulus responsive properties. *Adv. Mater.* **2008**, *20*, 2508−2511.

(10) Aggeli, A.; Bell, M.; Boden, N.; Keen, J. N.; Knowles, P. F.; McLeish, T. C. B.; Pitkeathly, M.; Radford, S. E. Responsive gels formed by the spontaneous self-assembly of peptides into polymeric β-sheet tapes. *Nature* **1997**, *386*, 259−262.

(11) Ihara, H.; Sakurai, T.; Yamada, T.; Hashimoto, T.; Takafuji, M.; Sagawa, T.; Hachisako, H. Chirality control of self-assembling organogels from a lipophilic L-glutamide derivative with metal chlorides. *Langmuir* **2002**, *18*, 7120−7123.

(12) Lam, S. T.; Yam, V. W.-W. Synthesis, characterisation and photophysical study of alkynylrhenium(I) tricarbonyl diimine complexes and their metal-Ion coordination-assisted metallogelation properties. *Chem.—Eur. J.* **2010**, *16*, 11588−11593.

(13) Estroff, L. A.; Hamilton, A. D. Water gelation by small organic molecules. *Chem. Rev.* **2004**, *104*, 1201−1218.

(14) George, M.; Weiss, R. G. In *Molecular Gels. Materials with Self-Assembled Fibrillar Networks*, Weiss, R. G., Terech, P., Eds.; Springer: Dordrecht, 2006; pp 449−551.

(15) Furmant, I.; Weiss, R. G. Factors influencing the formation of thermally reversible gels comprised of cholesteryl4-(2-anthryloxy)-butanoate in hexadecane, 1-octanol, or their mixtures. *Langmuir* **1993**, *9*, 2084−2088.
(16) Jung, J. H.; John, G.; Masuda, M.; Yoshida, K.; Shinkai, S.; Shimizu, T. Self-assembly of a sugar-based gelator in water: its remarkable diversity in gelation ability and aggregate structure. *Langmuir* **2001**, *17*, 7229−7232.
(17) Fujita, N.; Shinkai, S. In *Molecular Gels. Materials with Self-Assembled Fibrillar Networks*, Weiss, R. G., Térech, P., Eds.; Springer: Dordrecht, 2006; pp 562−570.
(18) Jadhav, S. R.; Vemula, P. K.; Kumar, R.; Raghavan, S. R.; John, G. Sugar-derived phase-selective molecular gelators as model solidifiers for oil spills. *Angew. Chem., Int. Ed.* **2010**, *49*, 7695−7698.
(19) Yan, N.; He, G.; Zhang, H. L.; Ding, L. P.; Fang, Y. Glucose-based fluorescent low-molecular mass compounds: creation of simple and versatile supramolecular gelators. *Langmuir* **2010**, *26*, 5909−5917.
(20) Reichwagen, J.; Hopf, H.; Guerzo, A. D.; Belin, C.; Bouas-Laurent, H.; Desvergne, J.-P. Synthesis of 2,3-substituted tetracenes and evaluation of their self-assembling properties in organic solvents. *Org. Lett.* **2005**, *7*, 971−974.
(21) Kim, T. H.; Choi, M. S.; Sohn, B.-H.; Park, S.-Y.; Lyoo, W. S.; Lee, T. S. Gelation-induced fluorescence enhancement of benzoxazole-based organogel and its naked-eye fluoride detection. *Chem. Commun.* **2008**, 2364−2366.
(22) Yang, H.; Yi, T.; Zhou, Z. G.; Zhou, Y. F.; Wu, J. C.; Xu, M.; Li, F. Y.; Huang, C. H. Switchable fluorescent organogels and mesomorphic superstructure based on naphthalene derivatives. *Langmuir* **2007**, *23*, 8224−8230.
(23) Hansen, C. M. *Hansen solubility parameters. A user' s handbook*, 2nd ed.; CRC Press: Boca Raton, FL, 2007.
(24) Appaw, C.; Gilbert, R. D.; Khan, S. A. Viscoelastic behavior of cellulose acetate in a mixed solvent system. *Biomacromolecules* **2007**, *8*, 1541−1547.
(25) Raynalab, M.; Bouteiller, L. Organogel formation rationalized by Hansen solubility parameters. *Chem. Commun.* **2011**, *47*, 8271−8273.
(26) Gao, J.; Wu, S.; Rogers, M. A. Harnessing Hansen solubility parameters to predict organogel formation. *J. Mater. Chem.* **2012**, *22*, 12651−12658.
(27) Yang, M.; Yan, N.; He, G.; Liu, T.; Fang, Y. Synthesis and gelation behavior of a pyrene-containing glucose derivative. *Acta. Phys. -Chim. Sin.* **2009**, *25*, 1040−1046.
(28) Yaws, C. L.; Leh, A. S. Y. In *Thermophysical Properties of Chemicals and Hydrocarbons*, Yaws, C. L., Ed.; William Andrew: Norwich, 2008, pp 649−658.
(29) George, M.; Funkhouser, G. P.; Weiss, R. G. Organogels with complexes of ions and phosphorus-containing amphiphiles as gelators. Spontaneous gelation by in situ complexation. *Langmuir* **2008**, *24*, 3537−3544.
(30) Developed using *MATLAB* Compiler Runtime (MathWorks) as a platform. Available upon request from Kevin Diehn.
(31) Bondi, A. van der Waals volumes and radii. *J. Phys. Chem.* **1964**, *68*, 441−451.
(32) Pfannemüller, B.; Welte, W. Amphiphilic properties of synthetic glycolipids based on amide linkages. I. Electron microscopic studies on aqueous gels. *Chem. Phys. Lipids* **1985**, *37*, 227−240.
(33) Bhuniya, S.; Kim, B. H. An insulin-sensing sugar-based fluorescent hydrogel. *Chem. Commun.* **2006**, 1842−1844.
(34) Fuhrhop, J. H.; Schnieder, P.; Boekema, E.; Helfrich, W. Lipid bilayer fibers from diastereomeric and enantiomeric N-octylaldonamides. *J. Am. Chem. Soc.* **1988**, *110*, 2861−2867.
(35) Although we cannot state with certainty what is the nature of the extraneous material in the Series A materials, a glucono-derived species seems most likely based on the elemental analyses and spectral evidence.
(36) Cai, X.; Liu, K.; Yan, J.; Zhang, H.; Hou, X.; Liu, Z.; Fang, Y. Calix[4]arene-based supramolecular gels with unprecedented rheological properties. *Soft Matter* **2012**, *8*, 3756−3761.
(37) Xing, B. G.; Yu, C. W.; Chow, K. H.; Ho, P. L.; Fu, D. G.; Xu, B. Hydrophobic interaction and hydrogen bonding cooperatively confer a vancomycin hydrogel: A potential candidate for biomaterials. *J. Am. Chem. Soc.* **2002**, *124*, 14846−14847.
(38) Žinic, M.; Vögtle, F.; Fages, F. Cholesterol-based gelators. *Top. Curr. Chem.* **2005**, *256*, 39−76.
(39) Mallia, V. A.; Butler, P. D.; Sarkar, B.; Holman, T.; Weiss, R. G. Reversible phase transitions within self-assembled fibrillar networks of (R)-18-(n-alkylamino)octadecan-7-ols in their carbon tetrachloride gels. *J. Am. Chem. Soc.* **2011**, *133*, 15045−15054.
(40) Ostuni, E.; Kamaras, P.; Weiss, R. G. Novel X-ray method for in situ determination of gelator strand structure: polymorphism of cholesteryl anthraquinone-2-carboxylate. *Angew. Chem., Int. Ed.* **1996**, *35*, 1324−1326.
(41) Seo, S. H.; Chang, J. Y. Organogels from ^{1}H-imidazole amphiphiles: entrapment of a hydrophilic drug into strands of the self-assembled amphiphiles. *Chem. Mater.* **2005**, *17*, 3249−3254.
(42) Xue, P. C.; Lu, R.; Chen, G. J.; Zhang, Y.; Nomoto, H.; Takafuji, M.; Ihara, H. Functional organogel based on a salicylideneaniline derivative with enhanced fluorescence emission and photochromism. *Chem.—Eur. J.* **2007**, *13*, 8231−8239.
(43) Kar, T.; Debnath, S.; Das, D.; Shome, A.; Das, P. K. Organogelation and hydrogelation of low-molecular-weight amphiphilic dipeptides: pH responsiveness in phase-selective gelation and dye removal. *Langmuir* **2009**, *25*, 8639−8648.
(44) Ajayaghosh, A.; Praveen, V. K. π-Organogels of self-assembled p-phenylenevinylenes: Soft materials with distinct size, shape, and functions. *Acc. Chem. Res.* **2007**, *40*, 644−656.
(45) Häner, R.; Garo, F.; Wenger, D.; Malinovskii, V. L. Oligopyrenotides: abiotic, polyanionic oligomers with nucleic acid-like structural properties. *J. Am. Chem. Soc.* **2010**, *132*, 7466−7471.
(46) Yao, J. H.; Elder, K. R.; Guo, H.; Grant, M. Theory and simulation of Ostwald ripening. *Phys. Rev. B* **1993**, *47*, 14110−14125.
(47) Wang, C.; Wang, Z.; Zhang, D.; Zhu, D. Thermal modulation of the monomer/excimer fluorescence for bispyrene molecules through the gel−solution transition of an organogel: A thermo-driven molecular fluorescence switch. *Chem. Phys. Lett.* **2006**, *428*, 130−133.
(48) Kamikawa, Y.; Kato, T. Color-tunable fluorescent organogels: columnar self-assembly of pyrene-containing oligo(glutamic acid)s. *Langmuir* **2007**, *23*, 274−278.
(49) Unexpectedly, the shape of the excitation spectra of 1.5% P7 in acetonitrile were somewhat different in flattened capillaries with 0.4, 0.85, and 84 mm pathlengths (Figure S20a); the corresponding emission spectra differ as well, but to a smaller extent (Figure S20b). Although we cannot offer a good explanation for this phenomenon, we hypothesize that it is related to instrumental factors, i.e., the depth of the focused excitation beam within the samples or even enhanced surface effects in the narrowest samples. Additional studies will be necessary to understand these differences.
(50) Castanheira, E. M. S.; Martinho, J. M. G. Solvatochromic shifts of pyrene excimer fluorescence. *Chem. Phys. Lett.* **1991**, *185*, 319−323.
(51) Dong, D. C.; Winnik, M. A. The Py scale of solvent polarities. *Can. J. Chem.* **1984**, *62*, 2560−2565.
(52) Ezzell, S. A.; McCormick, C. L. Water-soluble copolymers. 39. Synthesis and solution properties of associative acrylamido copolymers with pyrenesulfonamide fluorescence labels. *Macromolecules* **1992**, *25*, 1881−1886.
(53) Piłakowska-Pietras, D.; Lunkenheimer, K.; Piasecki, A.; Pietras, M. Adsorption behavior of surface chemically pure N-cycloalkylaldonamides at the air/water interface. *Langmuir* **2005**, *21*, 4016−4023.
(54) Noponen, V.; Nonappa; Lahtinen, M.; Valkonen, A.; Salo, H.; Kolehmainen, E.; Sievanen, E. Bile acid-amino acid ester conjugates: gelation, structural properties, and thermoreversible solid to solid phase transition. *Soft Matter* **2010**, *6*, 3789−3796.
(55) Gharagheizi, F. New procedure to calculate the Hansen solubility parameters of polymers. *J. Appl. Polym. Sci.* **2007**, *103*, 31−36.
(56) Yao, S.; Beginn, U.; Gress, T.; Lysetska, M.; Würthner, F. Supramolecular polymerization and gel formation of bis(Merocyanine)

dyes driven by dipolar aggregation. *J. Am. Chem. Soc.* **2004**, *126*, 8336−8348.
(57) Peng, J. X.; Liu, K. Q.; Liu, J.; Zhang, Q. H.; Feng, X. L.; Fang, Y. New dicholesteryl-based gelators: chirality and spacer length effect. *Langmuir* **2008**, *24*, 2992−3000.
(58) Weng, W. G.; Beck, J. B.; Jamieson, A. M.; Rowan, S. J. Understanding the mechanism of gelation and stimuli-responsive nature of a class of metallo-supramolecular gels. *J. Am. Chem. Soc.* **2006**, *128*, 11663−11672.

Supporting Information

for

Pyrenyl-Linker-Glucono Gelators. Correlations of Gel Properties with Gelator Structures and Characterization of Solvent Effects

Ni Yan,[†,‡] Zhiyan Xu,[†] Kevin K. Diehn,[§] Srinivasa R. Raghavan,[§] Yu Fang,[*,†] and Richard G. Weiss[*,‡]

[†]Key Laboratory of Applied Surface and Colloid Chemistry (Ministry of Education), School of Chemistry and Chemical Engineering, Shaanxi Normal University, Xi'an 710062, P. R. China

[‡]Department of Chemistry, Georgetown University, Washington, D.C. 20057-1227, United States

[§]Department of Chemical and Biomolecular Engineering, University of Maryland, College Park, MD 20742-2111, United States

Table of Contents

[*] To whom correspondence should be addressed. E-mail: yfang@snnu.edu.cn (YF), weissr@georgetown.edu (RGW).

1. Syntheses of glucono-based pyrenyl-containing compounds

Materials: 1,3-Propanediamine (99+%), 1,4-butanediamine (99%), 1,7-heptanediamine (99%), 1,8-octanediamine (99%), and D-glucono-1,5-lactone (99%) were purchased from Alfa Aesar and used as received. Pyrene (Acros, 96%) was recrystallized from ethanol and then extracted with ethanol in a Soxhlet extractor. 1,2-Ethylenediamine (analytical grade) was treated with solid KOH and distilled before use. All solvents and other chemicals used for syntheses were analytical grade and were purifiedby standard literature methods.

These compounds **P2**-**P8**, which are the final gelators with spacers containing 1,2-ethylenediamine, 1,3-propanediamine, 1,4-butanediamine, 1,6-hexanediamine, 1,7-heptanediamine, and 1,8-octanediamine, respectively, were synthesized by adopting literature methods as described below (Scheme S1).[1-3]

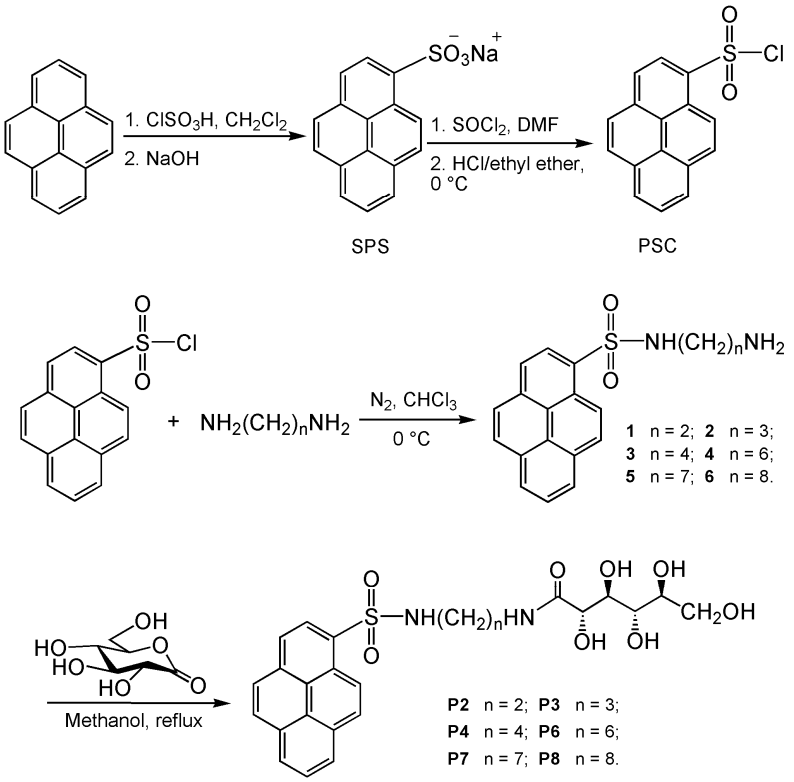

Scheme S1. Synthesis of glucono-appended pyrenyl derivatives (**Pn**).

(a) Synthesis of Sodium Pyrene-1-sulfonate (SPS):

Pyrene (4.85 g, 0.0240 mol) was dissolved in CH_2Cl_2 (30 mL). Chlorosulfonic acid (1.60 mL, 0.0240 mol), dissolved in CH_2Cl_2 (5 mL), was added drop-wise to the pyrene solution while stirring vigorously at 0 °C under a nitrogen atmosphere. Stirring was continued for a total of 2 h. The resulting dark-green solution was poured (*with extreme caution*) into ice (50 cm^3) and stirred in a beaker, allowing CH_2Cl_2 to evaporate in air at room temperature over a 2-day period. This solution was filtered twice through celite and the celite pad was washed with H_2O (100 mL). The yellow sodium salt of SPS was precipitated upon addition of NaOH (1.00 g, 0.0250 mol) to the filtrate. The solid was filtered and vacuum-dried (~ 1000 Pa) at 65 °C to yield 5.20 g (71%) of SPS sodium salt which was used in subsequent reactions without further purification.

(b) Synthesis of Pyrene-1-sulfonyl Chloride (PSC):

Hydrogen chloride was generated by adding concentrated sulfuric acid to sodium chloride and was dried by passing the gas through concentrated sulfuric acid before bubbling it through diethyl ether. The concentration of dissolved HCl, ~1 mol/L, was determined by adding 1 mL of the HCl/diethyl ether solution to ca. 10 mL of water followed by titration with a standard sodium hydroxide solution and phenolphthalein as the indicator. A 30 mL aliquot of the HCl/diethyl ether solution was added to a solution of SPS (9.10 g, 0.0300 mol) in DMF (200 mL) to generate the sulfonic acid. Thionyl chloride (22 mL, 0.180 mol) was then added dropwise under a nitrogen atmosphere. The reaction mixture was placed in an ice-water bath (~5 °C) for 3 h, and then the solution was poured into ice (400 cm^3). The yellow precipitate was filtered and washed with H_2O (500 mL). The solid was air-dried overnight then vacuum-dried (~ 1000 Pa) at 55 °C for 12 h. The crude PSC was passed through a silica gel column with CH_2Cl_2 as eluent (R_f = 0.85) to yield 7.20 g (yield 80%) of PSC. Elemental analysis (EA) (%) calcd for PSC $C_{16}H_9SO_2Cl$: C, 63.89; H, 3.00. Found: C, 63.60; H, 2.99.

(c) Syntheses of *N*-(1-Pyrenylsulfony1)alkyldiamines (**1**-**6**):

The *N*-(1-pyrenylsulfonyl)alkyldiamines were prepared from PSC and one of 1,2-ethylenediamine, 1,3-propanediamine, 1,4-butanediamine, 1,6-hexanediamine, 1,7-heptanediamine, or 1,8-octanediamine.

1,2-Ethylenediamine (4.50 mL, 0.0670 mol) was added to $CHCl_3$ (50 mL) and stirred rapidly at 0 °C under a nitrogen atmosphere. PSC (2.00 g, 6.60 mmol) was dissolved in $CHCl_3$ (300 mL) and added dropwise to the stirred diamine solution. After addition was completed (about 8 h), the mixture was brought to room temperature and stirred for another 2 h. The $CHC1_3$ layer was extracted with H_2O

(6x200 mL) and 5% aqueous NaCl (250 mL), dried over anhydrous sodium sulfate, and filtered. The filtrate was evaporated under reduced pressure and the residue was dried in vacuum (~1000 Pa) to give **1** as a yellow solid (1.87 g, 80%). The procedures used for the preparation of **2-6** were similar to that for **1**. The yields for **2-6** were 75%, 78%, 75%, 80% and 70%, respectively.

(d) Syntheses of **P2**-**P8**:

D-glucono-1,5-lactone (0.940 g, 5.30 mmol) and compound **1** (1.72 g, 5.30 mmol) were dissolved in methanol (200 mL), and the mixture was stirred and refluxed in air for 10 h. The residue obtained after the solvent was removed by evaporation was washed with chloroform (6x50 mL) to remove unreacted compound **1** and with water (6x50 mL) to remove unreacted lactone or species derived from it. The remaining solid was dried in vacuum (~1000 Pa) to give a yellow powder (1.60 g, 60% yield), **P2**. Analogous procedures were used for the preparations of **P3**, **P4**, **P6, P7** and **P8**. However, the purification procedures for **P4**, **P6, P7** and **P8** were somewhat different.

To purify **P4**, 100 mL of water were added to the residue which had been washed with $CHCl_3$; the mixture became a very viscous suspension which could not be filtered. NaCl solid (1 wt % of the coarse **P4**) was added to this suspension followed by centrifugation of the mixture at ~10,000 rpm for 30 min. The supernatant liquid was removed and the solid was treated as above with aqueous NaCl 7 more times; between each centrifugation, the solid was collected and stirred in an aqueous NaCl solution for 30 min. Finally, the solid was washed with water, centrifuged and dried in vacuum (~1000 Pa) to give **P4** as a yellow powder (1.68 g, 56% yield). The procedures for the purification of **P6, P7** and **P8** are similar to that for **P4**.

For **P2**: 60% yield. mp 173.5-175 ºC. ^{1}H NMR (DMSO-d_6/Me_4Si, 300 MHz) δ (ppm): 8.97-9.00 (d, J = 9 Hz, 1H), 8.59-8.61 (d, J = 6 Hz, 1H), 8.20-8.50 (m, 8H), 7.75 (s, 1H), 5.33 (s, 1H), 4.30-4.52 (m, 4H), 3.86-3.92 (d, 2H), 3.45-3.55 (m, 4H), 3.10 (s, 2H), 2.88 (s, 2H). ^{13}C NMR (DMSO-d_6/Me_4Si, 100 MHz): δ 173.19 (1C, CO), 134.40, 132.69, 130.96, 130.40, 130.12, 129.98, 127.57, 127.54, 127.45, 127.37, 127.27, 127.15, 124.73, 124.67, 123.75, 123.61 (16C, ArC), 73.86, 72.69, 71.88, 70.39, 63.74 (5C, COH), 42.23, 38.61 (2C, CH_2). FTIR (KBr) υ_{max} (cm^{-1}): 3407 (NH), 3533-3045 (OH); 3380 ($HNSO_2$); 2927 (CH); 1652 (C=O); 1533 (NH); 1415 (CN); 1309, 1151 (S=O). EA (%) calcd for $C_{24}H_{26}N_2O_8S\cdot\frac{1}{2}H_2O$: C, 56.35; H, 5.32; N, 5.48. Found: C, 56.75; H, 5.11; N, 5.37.

For **P3**: 65% yield. mp 167-168.5 ºC. ^{1}H NMR (DMSO-d_6/Me_4Si, 300 MHz) δ (ppm): 8.97-9.00 (d, J = 9 Hz, 1H), 8.59-8.61 (d, J = 6 Hz, 1H), 8.19-8.50 (m, 7H), 8.10 (s, 1H), 7.63 (s, 1H), 5.33 (s, 1H), 4.32-4.54 (m, 4H), 3.87-3.95 (m, 2H), 3.38-3.56 (m, 4H), 3.00-3.01 (t, J = 3 Hz 2H), 2.51-2.86 (t, J = 6 Hz, 2H), 1.45-1.49 (t, J = 6 Hz, 2H). ^{13}C NMR (DMSO-d_6/Me_4Si, 100 MHz): δ 172.97 (1C, CO), 134.32, 133.09, 130.97, 130.33, 130.13, 129.89, 127.56, 127.50, 127.41, 127.38, 127.24, 127.06, 124.73, 124.68, 123.83, 123.63 (16C, ArC), 73.98, 72.80, 71.93, 70.47, 63.75 (5C, COH), 42.22, 35.99, 29.82 (3C, CH_2). FTIR (KBr) υ_{max} (cm^{-1}): 3405 (NH), 3590-3050 (OH); 3396 ($HNSO_2$); 2933 (CH); 1646 (C=O); 1548 (NH); 1438 (CN); 1311, 1149 (S=O). EA (%) calcd for $C_{25}H_{28}N_2O_8S\cdot\frac{1}{2}H_2O$: C, 57.13; H, 5.56; N, 5.33. Found: C, 57.07; H, 5.35; N, 5.31.

For **P4**: 56% yield. mp 131.8-133.5 ºC. ^{1}H NMR (DMSO-d_6/Me_4Si, 300 MHz) δ (ppm): 9.01-9.04 (d, J = 9 Hz, 1H), 8.60-8.62 (d, J = 6 Hz, 1H), 8.19-8.50 (m, 7H), 8.12 (s, 1H), 7.57 (s, 1H), 5.35 (s, 1H), 4.38-4.59 (m, 4H), 3.90-3.97 (m, 2H), 3.42-3.62 (m, 4H), 2.84-2.96 (b, 4H), 1.35-1.46 (b, 4H). ^{13}C NMR (DMSO-d_6/Me_4Si, 100 MHz): δ 172.71 (1C, CO), 134.29, 133.03, 130.95, 130.29, 130.12, 129.84, 127.53, 127.37, 127.20, 127.10, 127.05, 124.71, 124.63, 124.31, 123.90, 123.62 (16C, ArC), 74.04, 72.84, 71.92, 70.48, 63.78 (5C, COH), 42.57, 37.94, 26.85, 26.63 (4C, CH_2). FTIR (KBr) υ_{max} (cm^{-1}): 3408 (NH), 3600-3072 (OH); 3380 ($HNSO_2$); 2935 (CH); 1639 (C=O); 1542 (NH); 1438 (CN); 1307, 1141 (S=O). EA (%) calcd for $C_{26}H_{30}N_2O_8S\cdot\frac{1}{2}H_2O$: C, 57.87; H, 5.79; N, 5.19. Found: C, 57.30; H, 5.67; N, 5.30.

For **P6**: 60% yield. mp 127.0-129.5 ºC. ^{1}H NMR (DMSO-d_6/Me_4Si, 300 MHz) δ (ppm): 9.01-9.04 (d, J = 9 Hz, 1H), 8.60-8.63 (d, J = 9 Hz, 1H), 8.19-8.49 (m, 7H), 8.11 (s, 1H), 7.48 (s, 1H), 5.36 (s, 1H), 4.38-4.58 (m, 4H), 3.90-3.97 (m, 2H), 3.50-3.60 (m, 4H), 2.52-2.88 (b, 4H), 0.96-1.27 (m, 8H). ^{13}C NMR (DMSO-d_6/Me_4Si, 100 MHz): δ 172.56 (1C, CO), 134.30, 133.14, 130.95, 130.30, 130.13, 129.81, 127.54, 127.38, 127.21, 127.13, 127.06, 124.72, 124.62, 124.32, 123.92, 123.62 (16C, ArC), 74.03, 72.84, 71.91, 70.50, 63.80 (5C, COH), 42.71, 38.40, 29.40, 29.31, 26.11, 26.01 (6C, CH_2). FTIR (KBr) υ_{max} (cm^{-1}): 3410 (NH), 3595-3045 (OH); 3375 ($HNSO_2$); 2925 (CH); 1629 (C=O); 1544 (NH); 1425 (CN); 1311, 1141 (S=O). EA (%) calcd for $C_{28}H_{34}N_2O_8S\cdot\frac{1}{2}H_2O$: C, 59.24; H, 6.21; N, 4.93. Found: C, 59.92; H, 6.09; N, 4.98.

For **P7**: 55% yield. mp 139.9-142.4 ºC. ^{1}H NMR (DMSO-d_6/Me_4Si, 300 MHz) δ (ppm): 9.00-9.03 (d, J = 9 Hz, 1H), 8.59-8.61 (d, J = 6 Hz, 1H), 8.20-8.48 (m, 7H), 8.10 (s, 1H), 7.46 (s, 1H), 5.35 (s, 1H), 4.35-4.58 (m, 4H), 3.90-3.97 (m, 2H), 3.38-3.60 (m, 4H), 2.80-2.82 (b, 4H), 0.85-1.24 (m, 10H). ^{13}C

NMR (DMSO-d_6/Me_4Si, 100 MHz): δ 172.53 (1C, CO), 134.32, 133.17, 130.96, 130.30, 130.13, 129.80, 127.55, 127.39, 127.21, 127.15, 127.06, 124.73, 124.59, 124.32, 123.93, 123.63 (16C, ArC), 74.02, 72.85, 71.91, 70.51, 63.80 (5C, COH), 42.66, 38.47, 29.29, 29.26, 28.48, 26.48, 26.16 (7C, CH_2). FTIR (KBr) υ_{max} (cm^{-1}): 3419 (NH), 3590-3050 (OH); 3375 ($HNSO_2$); 2929 (CH); 1625 (C=O); 1544 (NH); 1430 (CN); 1308, 1141 (S=O). EA (%) calcd for $C_{29}H_{36}N_2O_8S\cdot\frac{1}{2}H_2O$: C, 59.88; H, 6.41; N, 4.82. Found: C, 59.71; H, 6.27; N, 4.94.

For **P8**: 50% yield. mp 141.1-144.3ºC. ^{1}H NMR (DMSO-d_6/Me_4Si, 300 MHz) δ (ppm): 9.00-9.03 (d, J = 9 Hz, 1H), 8.59-8.62 (d, J = 9 Hz, 1H), 8.19-8.48 (m, 7H), 8.05 (s, 1H), 7.45 (s, 1H), 5.32 (s, 1H), 4.32-4.52 (m, 4H), 3.91-3.97 (m, 2H), 3.41-3.59 (m, 4H), 2.82-2.81 (b, 4H), 0.77-1.19 (m, 12H). ^{13}C NMR (DMSO-d_6/Me_4Si, 100 MHz): δ 172.55 (1C, CO), 134.33, 133.20, 130.97, 130.31, 130.13, 129.78, 127.54, 127.39, 127.20, 127.17, 127.05, 124.73, 124.57, 124.33, 123.94, 123.63 (16C, ArC), 74.04, 72.86, 71.93, 70.54, 63.82 (5C, COH), 42.60, 38.55, 29.37, 29.16, 28.88, 28.66, 26.51, 26.10 (8C, CH_2). FTIR (KBr) υ_{max} (cm^{-1}): 3410 (NH), 3525-3050 (OH); 3370 ($HNSO_2$); 2921 (CH); 1637 (C=O); 1540 (NH); 1427 (CN); 1311, 1139 (S=O). EA (%) calcd for $C_{30}H_{38}N_2O_8S\cdot\frac{1}{2}H_2O$: C, 60.49; H, 6.60; N, 4.70. Found: C, 60.47; H, 6.41; N, 4.82.

(e) Further purification of **P4**-**P8**:

The **P4**-**P8** obtained using above-mentioned method are denoted as Series A. Aliquots were purified further, as described in detail for **P4**. **P4** (100 mg) was added to 1 mL of methanol and heated in a water bath until the solid dissolved. After cooling to room temperature, a very stable gel formed. The gel was destroyed mechanically with a glass rod, the liquid was removed with a pipette, the solid was washed with cold methanol, and the solid was collected by filtration. This process was repeated 3 times. Finally, the obtained solid was dried under vacuum (~3000 Pa) at 40 ºC for 48 h. The **P4**-**P8** aliquots purified with methanol are designated as Series B. The melting points and the elemental analyses of the **P4**-**P8** of both series are summarized in Table S1.

Table S1. Melting points and elemental analyses (EA) of **Pn** obtained by different protocols.

Pn	Series	Protocol and EA	Melting point (ºC)	C%	H%	N%
P2	A	Washed with water	173.5-175.0	56.75	5.11	5.37
		EA calcd. for $C_{24}H_{26}N_2O_8S•½H_2O$		56.35	5.32	5.48
P3	A	Washed with water	167.0-168.5	57.07	5.35	5.31
		EA calcd. for $C_{25}H_{28}N_2O_8S•½H_2O$		57.13	5.56	5.33
P4	A	Centrifugation with water and NaCl	131.8-133.5	57.30	5.67	5.30
	B	Gel washed with methanol	132.0-134.0	57.82	5.77	5.19
		EA calcd. for $C_{26}H_{30}N_2O_8S•½H_2O$		57.87	5.79	5.19
P6	A	Centrifugation with water and NaCl	127.0-129.5	59.92	6.09	4.98
	B	Gel washed with methanol	128.7-130.5	59.65	6.20	4.95
		EA calcd. for $C_{28}H_{34}N_2O_8S•½H_2O$		59.24	6.21	4.93
P7	A	Centrifugation with water and NaCl	139.9-142.4	59.71	6.27	4.94
	B	Gel washed with methanol	140.0-142.5	59.93	6.39	4.85
		EA calcd. for $C_{29}H_{36}N_2O_8S•½H_2O$		59.88	6.41	4.82
P8	A	Centrifugation with water and NaCl	141.1-144.3	60.47	6.41	4.82
	B	Gel washed with methanol	142.0-144.5	60.48	6.50	4.73
		EA calcd. for $C_{30}H_{38}N_2O_8S•½H_2O$		60.49	6.60	4.70

2. T_{gel} values of 1-decanol gels as a function of P7 concentration.

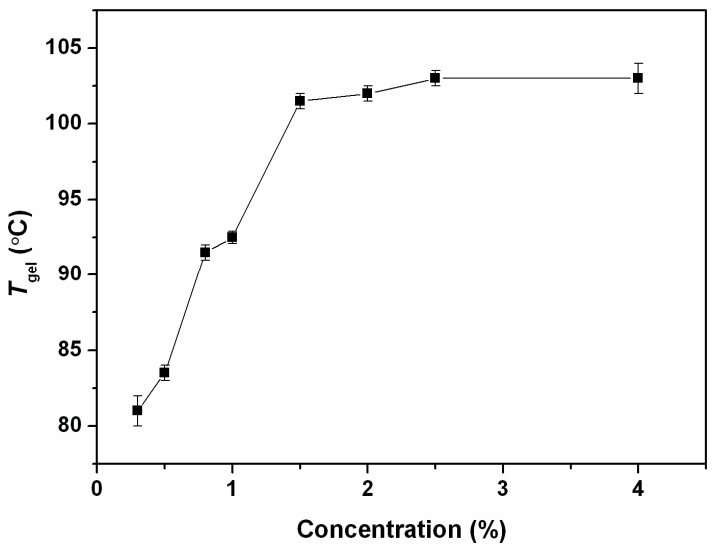

Figure S1. T_{gel} values of 1-decanol gels as a function of **P7** concentration. Temperature ranges of vertical bars refer to when the initial and final portions of a gel sample fell on being heated slowly in an inverted test tube.

3. Table of Hansen solubility parameters of the liquids examined and the CGCs of P3

Table S2. Hansen solubility parameters ($MPa^{0.5}$) of liquids examined, their distances (R) in Hansen space from **P3** (δ_p = 11.35 $MPa^{0.5}$, δ_h = 8.35 $MPa^{0.5}$, and δ_d = 17.25 $MPa^{0.5}$), and critical gelator concentrations (%) or appearances of **P3** in various liquids.

Species	Abbreviation	δ_p	δ_h	δ_d	δ	R	CGC (%) or appearance[a]
dimethyl sulfoxide	DMSO	16.40	10.20	18.40	26.68	5.85	S
dimethylformamide	DMF	13.70	11.30	17.40	24.86	3.78	S
pyridine	PYR	8.80	5.90	19.00	21.75	4.98	S
n-butylamine	NBA	4.50	8.00	16.20	18.62	7.17	S
tetrahydrofuran	THF	5.70	8.00	16.80	19.46	5.73	I
acetone	ACT	10.40	7.00	15.50	19.94	3.87	I
acetic acid	ACA	8.00	13.50	14.50	21.37	8.25	I
hexanoic acid	HXA	4.20	11.50	16.30	20.39	8.04	2.0
benzene	BNZ	0.00	2.00	18.40	18.51	13.21	I
toluene	TOL	1.40	2.00	18.00	18.16	11.90	I
cyclohexane	CHEX	0.00	0.20	16.80	16.80	14.00	I
n-nonane	NON	0.00	0.00	15.80	15.80	14.39	I
carbon tetrachloride	CTC	0.00	0.60	17.80	17.81	13.79	I
triethylamine	TEA	5.74	5.99	15.00	17.14	7.58	I
ethyl acetate	EAC	5.30	7.20	15.80	18.15	6.81	I
dichloromethane	DCM	6.30	6.10	18.20	20.20	5.85	I
chloroform	CHF	3.10	5.70	17.80	18.95	8.73	I
methanol	MOH	12.30	22.30	15.10	29.61	14.63	0.83
ethanol	EOH	8.80	19.40	15.80	26.52	11.71	0.83
1-propanol	POH	6.80	17.40	16.00	24.60	10.43	0.5
1-butanol	BOH	5.70	15.80	16.00	23.20	9.68	0.09
1-pentanol	PEOH	5.90	13.90	15.90	21.93	8.23	0.42
1-hexanol	HOH	5.80	12.50	15.90	21.04	7.44	0.2
1-heptanol	HPOH	5.30	11.70	16.00	20.52	7.35	0.08
1-octanol	OOH	3.30	11.90	17.00	21.01	8.81	0.42
1-nonanol	NOH	2.87	10.71	17.30	20.55	8.81	0.71

1-decanol	DOH	2.70	10.00	17.60	20.42	8.83	0.07
acetonitrile	ATN	18.00	6.10	15.30	24.40	8.03	I
diethyl ether	DEE	2.90	5.10	14.50	15.64	10.59	I
water	H2O	16.00	42.40	15.50	47.90	34.54	1.25

[a] [**P3**] = 2.5%, S = soluble, I = insoluble, Sus = suspension.

4. Hansen spaces of P2-P8 in liquids

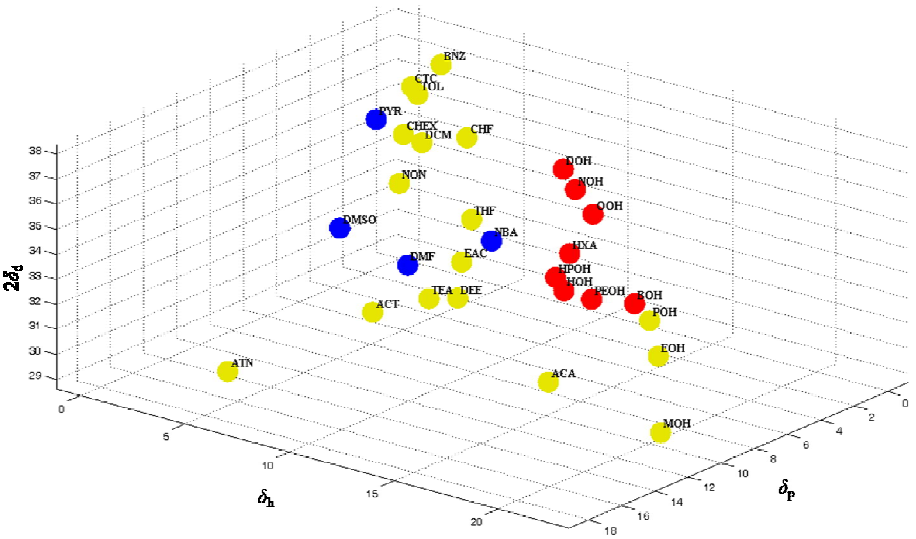

Figure S2. Solubility data for 2.5 % **P2** in neat liquids represented in Hansen space. Blue (soluble), red (gel), and yellow (insoluble). The datum point for water is not included; see text.

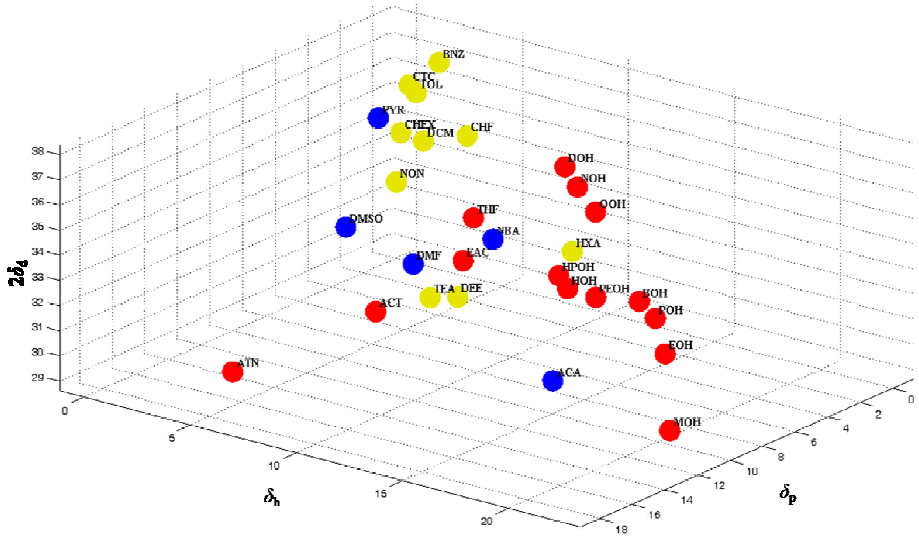

Figure S3. Solubility data for 2.5% **P4** in neat liquids represented in Hansen space. Blue (soluble), red (gel), and yellow (insoluble). The datum point for water is not included; see text.

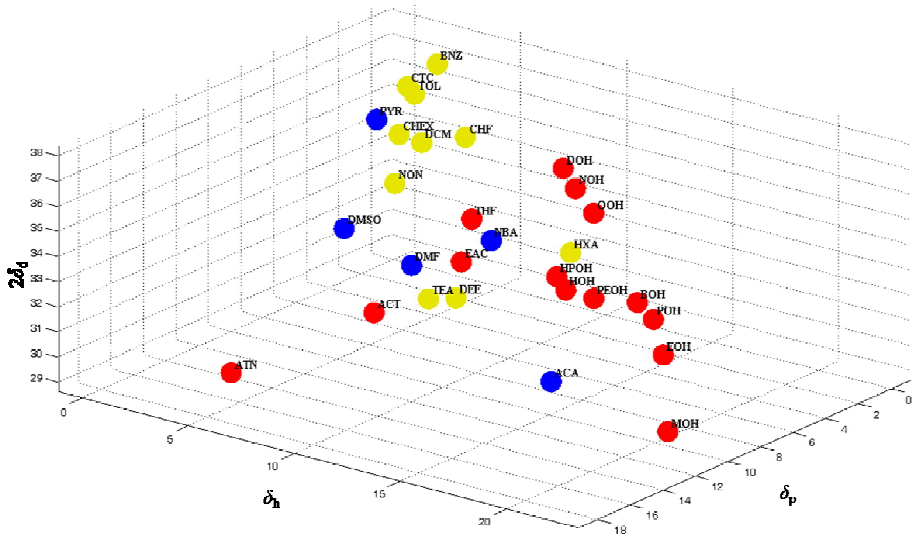

Figure S4. Solubility data for 2.5% **P6** in neat liquids represented in Hansen space. Blue (soluble), red (gel), and yellow (insoluble). The datum point for water is not included; see text.

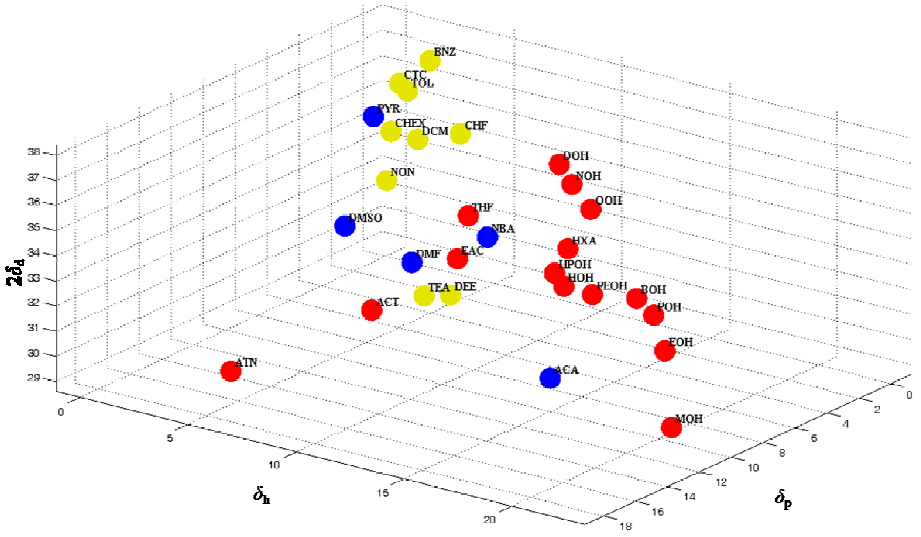

Figure S5. Solubility data for 2.5% **P7** in neat liquids represented in Hansen space. Blue (soluble), red (gel), and yellow (insoluble). The datum point for water is not included; see text.

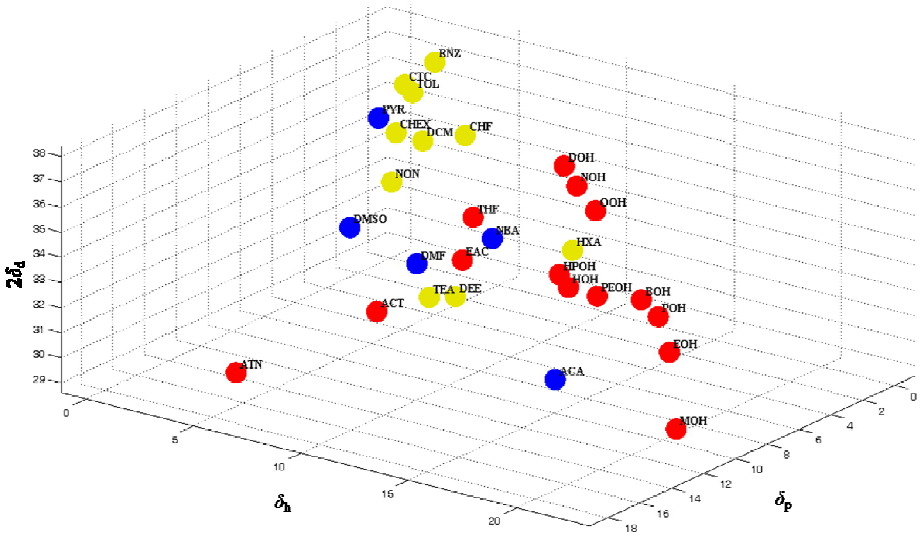

Figure S6. Solubility data for 2.5% **P8** in neat liquids represented in Hansen space. Blue (soluble), red (gel), and yellow (insoluble). The datum point for water is not included; see text.

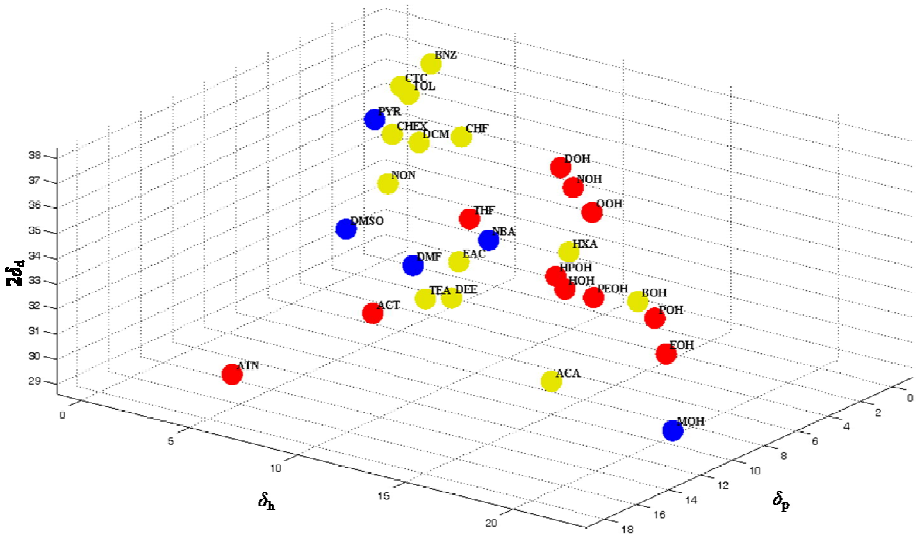

Figure S7. Solubility data for 2.5% **N3** in neat liquids represented in Hansen space. Blue (soluble), red (gel), and yellow (insoluble). The datum point for water is not included; see text.

5. Plots of CGCs of Pn as a function of HSPs

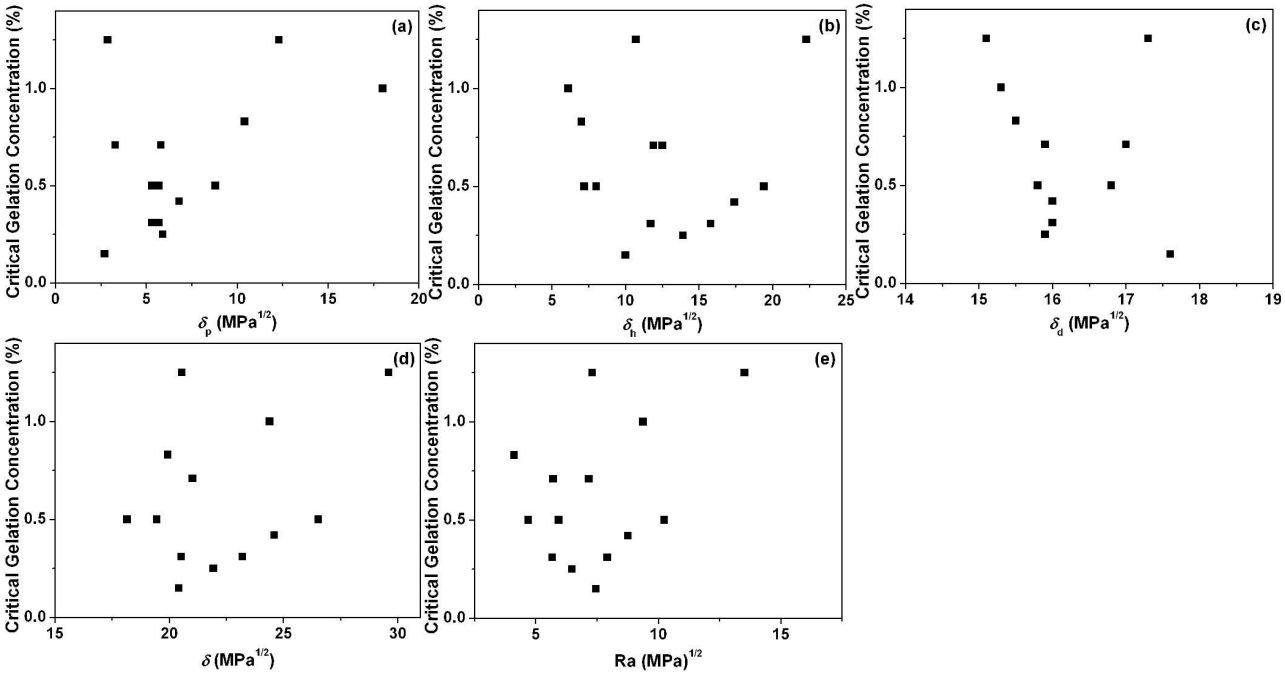

Figure S8. Critical gelation concentrations of **P4** in some liquids as a function of: (a) δ_p, (b) δ_h, (c) δ_d, (d) overall Hansen solubility parameter (δ), and (e) *R*a in Hansen space from **P4** (δ_p = 10.08 MPa$^{0.5}$, δ_h = 9.58 MPa$^{0.5}$, and δ_d = 17.1 MPa$^{0.5}$).

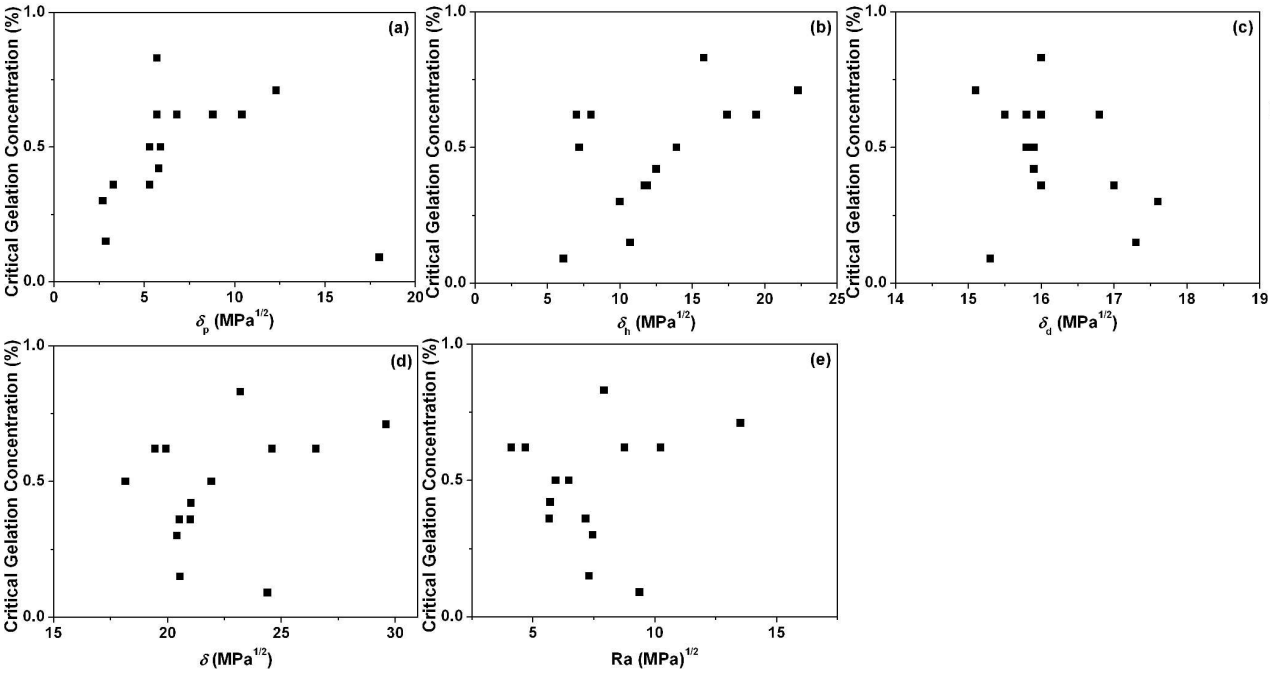

Figure S9. Critical gelation concentrations of **P6** in some liquids as a function of: (a) δ_p, (b) δ_h, (c) δ_d, (d) overall Hansen solubility parameter (δ), and (e) *R*a in Hansen space from **P6** (δ_p = 10.08 MPa$^{0.5}$, δ_h = 9.58 MPa$^{0.5}$, and δ_d = 17.1 MPa$^{0.5}$).

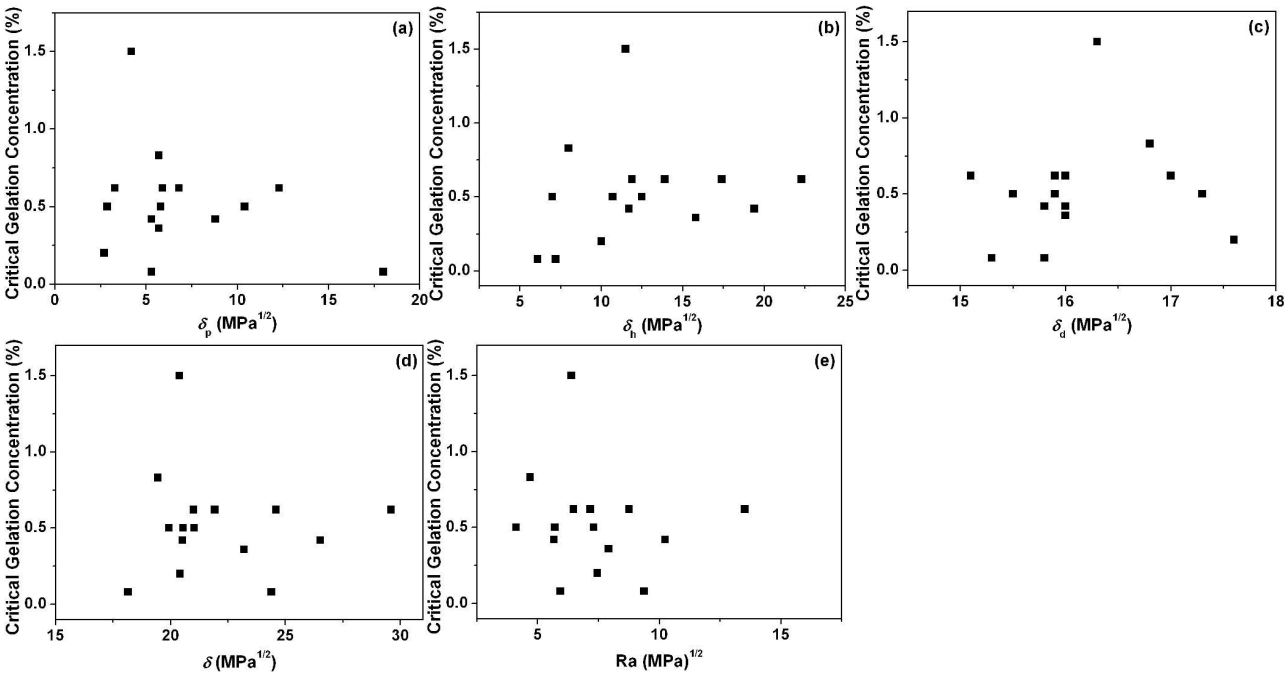

Figure S10. Critical gelation concentrations of **P7** in some liquids as a function of: (a) δ_p, (b) δ_h, (c) δ_d, (d) overall Hansen solubility parameter (δ), and (e) *R*a in Hansen space from **P7** (δ_p = 10.08 MPa$^{0.5}$, δ_h = 9.58 MPa$^{0.5}$, and δ_d = 17.1 MPa$^{0.5}$).

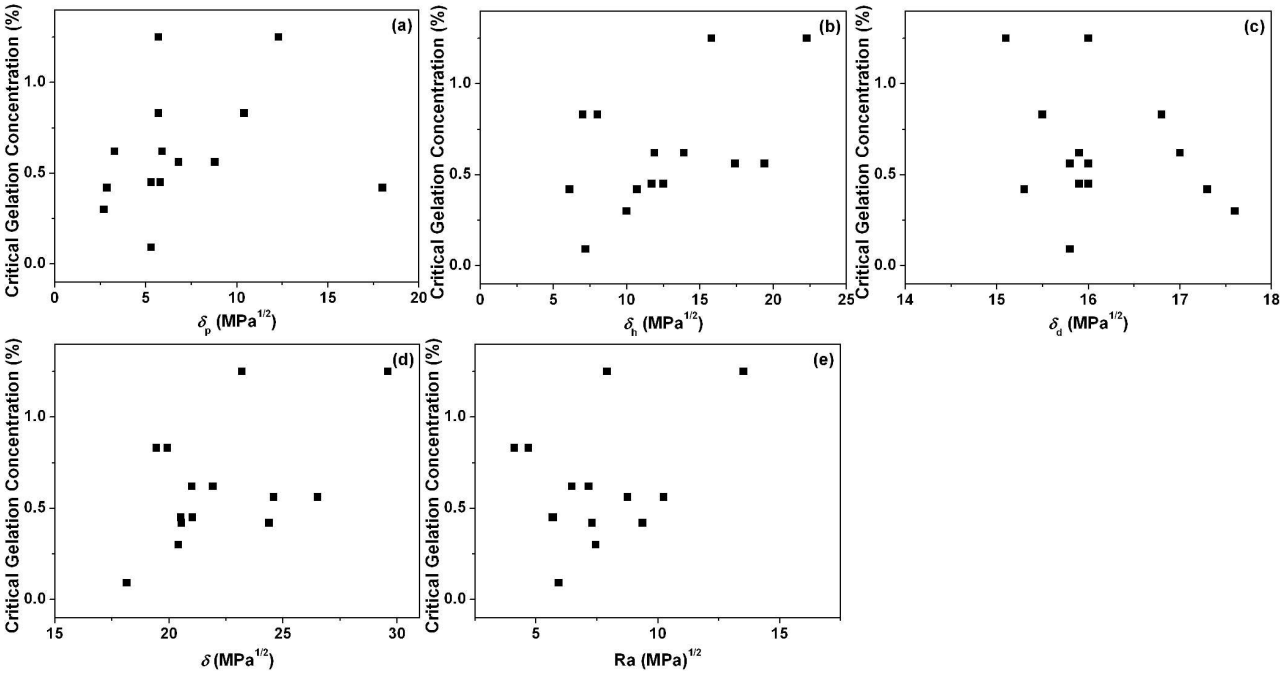

Figure S11. Critical gelation concentrations of **P8** in some liquids as a function of: (a) δ_p, (b) δ_h, (c) δ_d, (d) overall Hansen solubility parameter (δ), and (e) *R*a in Hansen space from **P8** (δ_p = 10.08 MPa$^{0.5}$, δ_h = 9.58 MPa$^{0.5}$, and δ_d = 17.1 MPa$^{0.5}$).

6. TEM image prepared from a dried 0.02% P7 in acetonitrile sol

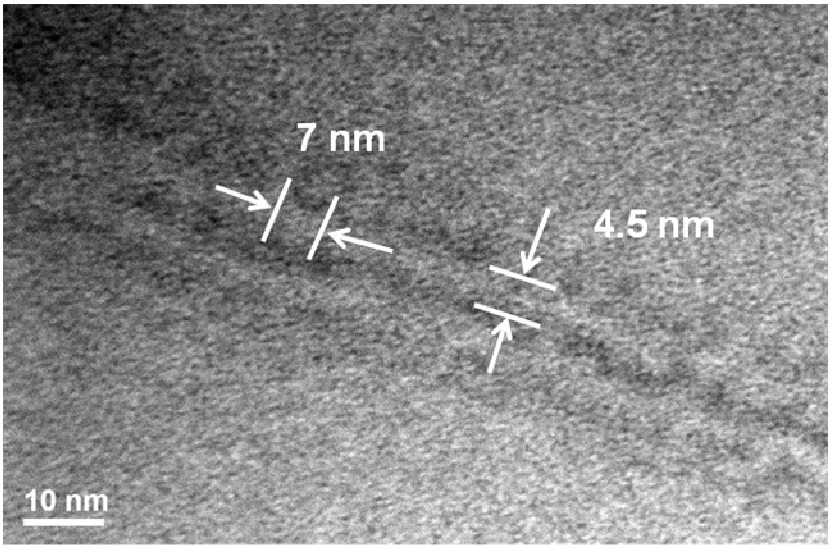

Figure S12. TEM image prepared from a dried 0.02% **P7** in acetonitrile sol.

7. Static contact angle (θ) measured on water for a xerogel film of P7 from acetonitrile

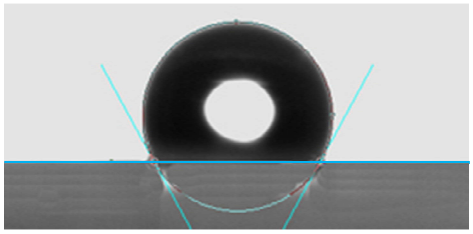

Figure S13. Droplet for static contact angle (θ) measurement on water for a xerogel film of **P7** from acetonitrile (Initial [**P7**] = 1.5%).

8. X-ray diffraction patterns of neat Pn and calculated extended molecular lengths

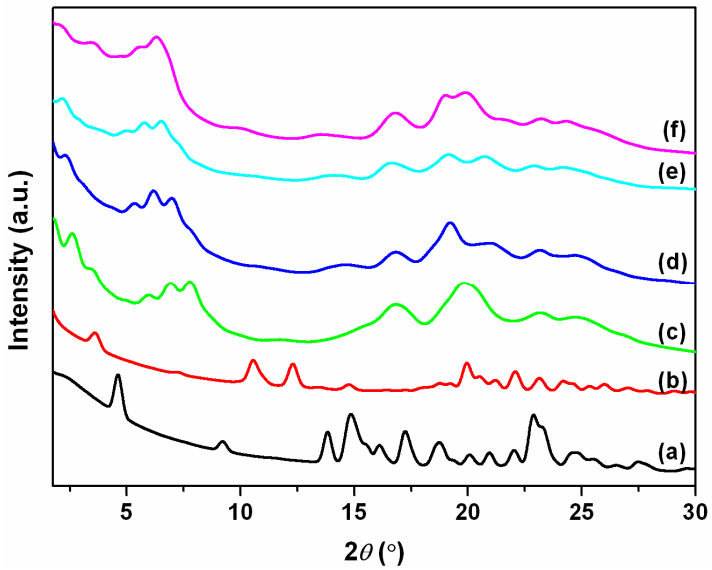

Figure S14. Vertically offset X-ray diffraction patterns of neat **Pn**. (a, b) **P2** and **P3** (Series A), (c-f) **P4**, **P6**, **P7** and **P8** (Series B), respectively.

Table S3. Comparison of the possible lattice types of the neat **Pn** after indexing the peaks in Figure S21, the *d* values of the diffraction peaks, and the calculated extended molecular lengths (*L*) of the **Pn**.

Pn	Possible lattice type	*d* (nm)	*L* (nm)
P2	hexagonal, orthorhombic, tetragonal	1.92, 0.96, 0.64, 0.59, 0.55, 0.51, 0.47, 0.44, 0.42, 0.40, 0.39, 0.38, 0.36	2.04
P3	monoclinic, orthorhombic	2.45, 1.23, 0.84, 0.72, 0.66, 0.60, 0.47, 0.46, 0.44, 0.43, 0.42, 0.40, 0.38	2.33,[3] 3.13
P4	monoclinic	3.41, 1.48, 1.28, 1.13, 0.53, 0.45, 0.38, 0.36	3.62
P6	monoclinic	3.87, 1.65, 1.43, 1.27, 0.61, 0.53, 0.46, 0.42, 0.38, 0.36	4.10
P7	monoclinic	4.16, 1.78, 1.54, 1.36, 0.62, 0.53, 0.46, 0.43, 0.39, 0.37	4.36
P8	monoclinic	4.43, 1.87, 1.60, 1.40, 0.65, 0.53, 0.47, 0.45, 0.43, 0.38	4.64

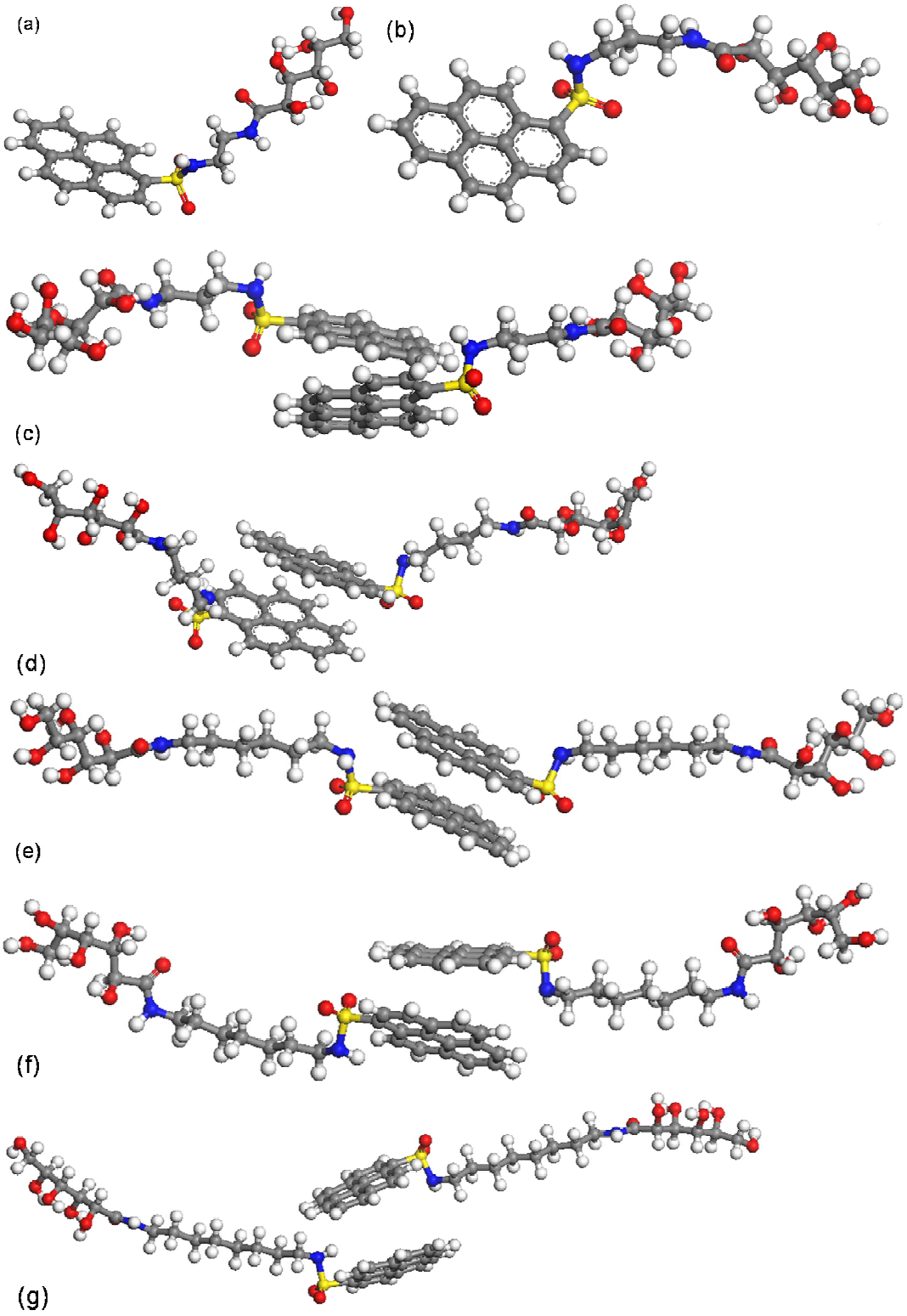

Figure S15. Energy-minimized extended molecular lengths of the **Pn** and their proposed packing arrangements (when interdigitated) and their calculated lengths: (a) **P2**, 2.04 nm, (b) **P3**, 2.33 nm,[3] (c) interdigitated **P3**, 3.13 nm, (d) interdigitated **P4**, 3.62 nm, (e) interdigitated **P6**, 4.10 nm, (d) interdigitated **P7**, 4.36 nm, and (g) interdigitated **P8**, 4.64 nm.

9. X-ray diffraction patterns of neat, xerogel and gel of P7

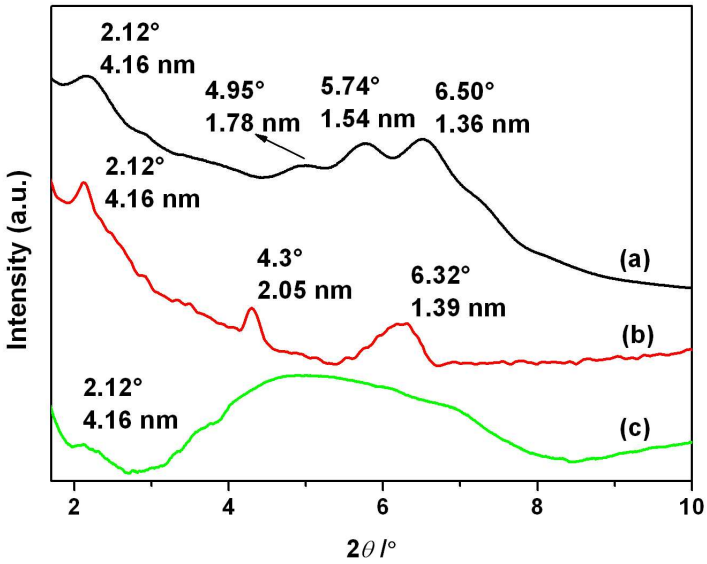

Figure S16. X-ray diffraction patterns of **P7** (Series B): (a) neat, (b) a xerogel from acetonitrile (initial [**P7**] = 2%), and (c) a 5% gel in acetonitrile after subtracting empirically the amorphous scattering of the acetonitrile liquid from the total gel diffractogram; see text for details.

10. The evolution of molecular packing of P7 in acetonitrile leading to gels

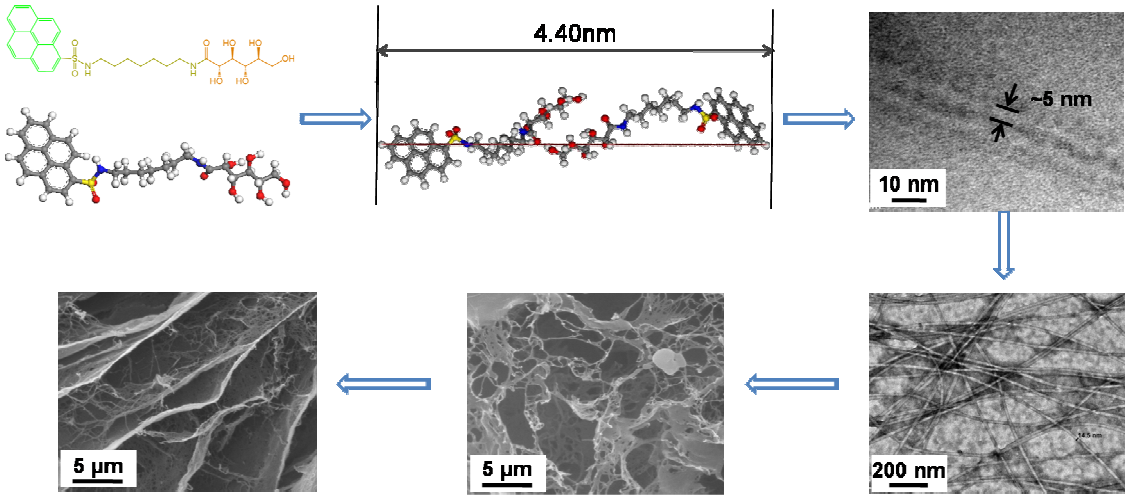

Scheme S2. Evolution of molecular aggregation of **P7** in acetonitrile leading to gels.

11. Reversible variation of the CD intensity at 295 nm between the sol and gel phases

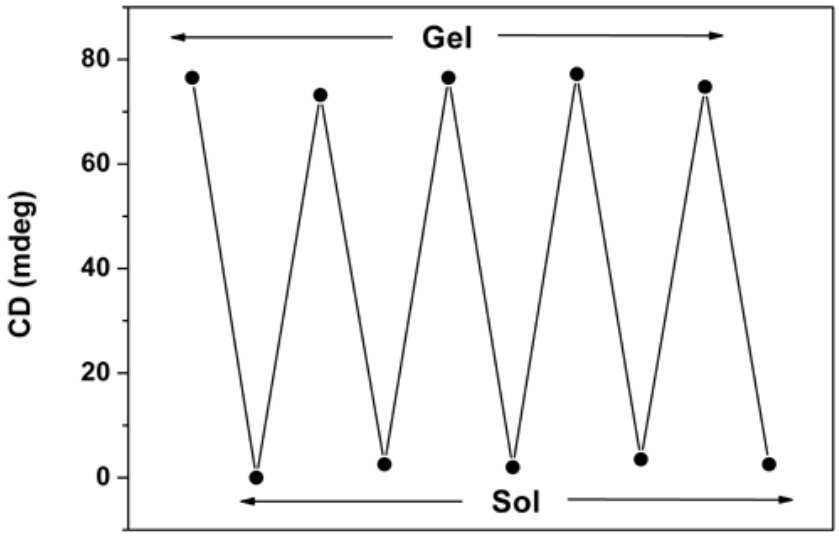

Figure S17. Reversibility of the CD intensity at 295 nm of 0.1 % **P7** in acetonitrile between the sol (55 °C) and gel (25 °C) phases.

12. Fluorescence excitation spectra of 1.5% P7 in acetonitrile

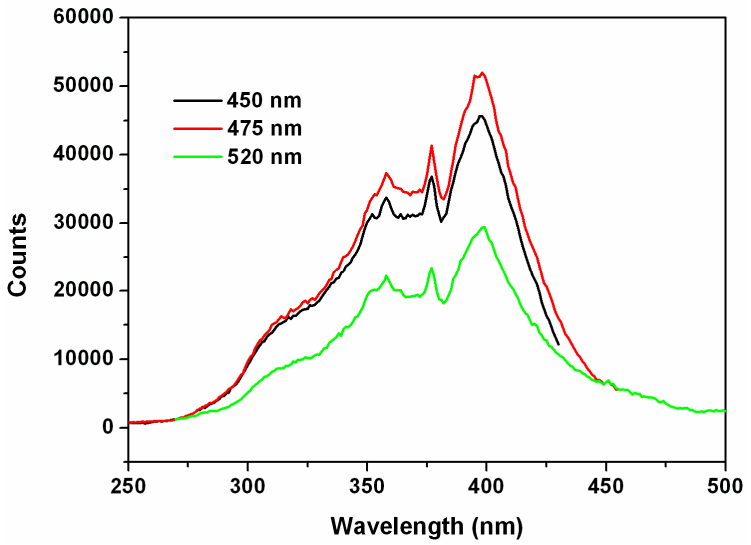

Figure S18. Fluorescence excitation spectra of a gel of 1.5% (2.6×10^{-2} M) **P7** (Series B) in acetonitrile at 20 °C at different emission wavelengths.

13. Fluorescence emission spectra of 1.5% P7 in acetonitrile

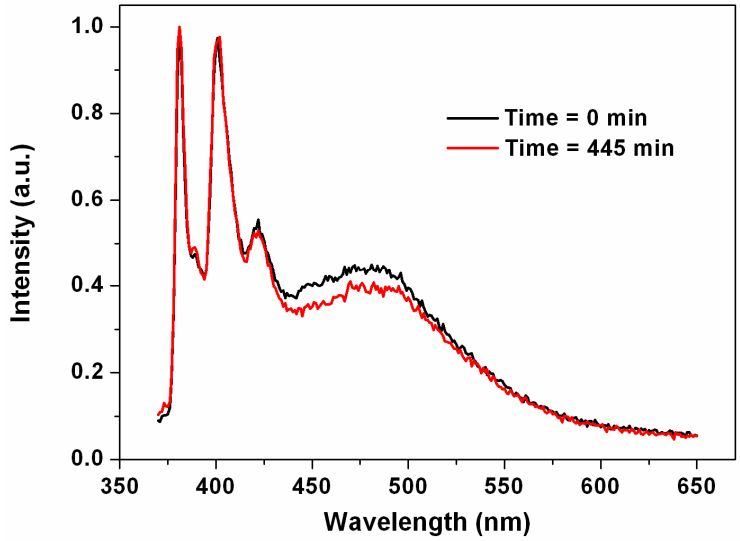

Figure S19. Fluorescence emission spectra (λ_{ex} 350 nm) of 1.5% (2.6×10^{-2} M) **P7** (Series B) in acetonitrile (20 °C) at ca. 0 and 445 min after gel preparation.

14. Fluorescence spectra of 1.5% P7 in in flattened capillaries with different pathlengths

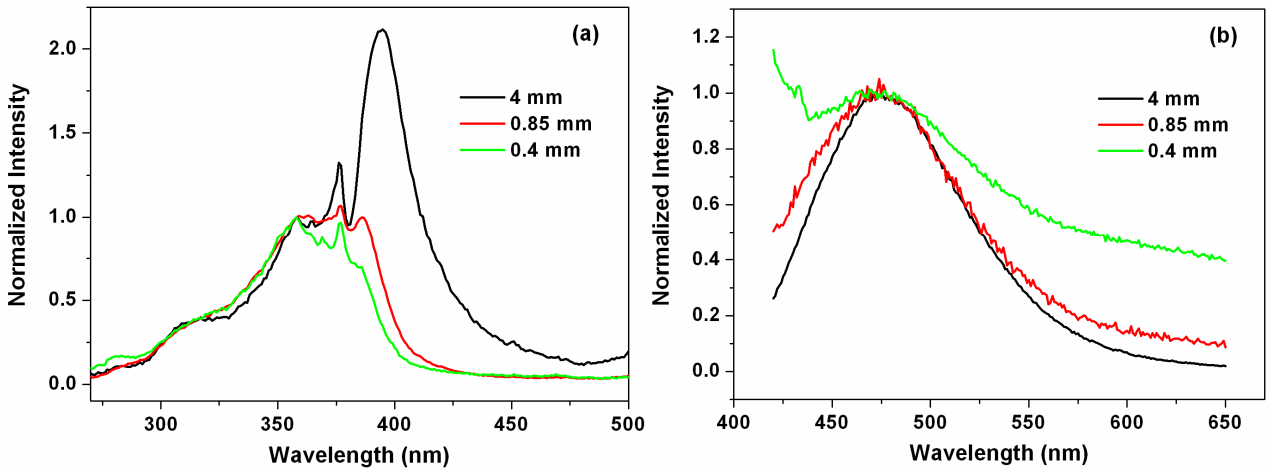

Figure S20. Fluorescence from 1.5% (2.6×10^{-2} M) **P7** (Series B) in acetonitrile in the gel phase (20 °C) in flattened capillaries with different pathlengths: (a) excitation spectra (λ_{em} 520 nm, normalized at 358 nm); (b) emission spectra (λ_{ex} 400 nm, normalized at 471 nm).

15. FTIR spectra of 8 mM P7 in DMF solution/sol, and P7/ethanol and P7/acetonitrile xerogels (initial [P7] = 2%)

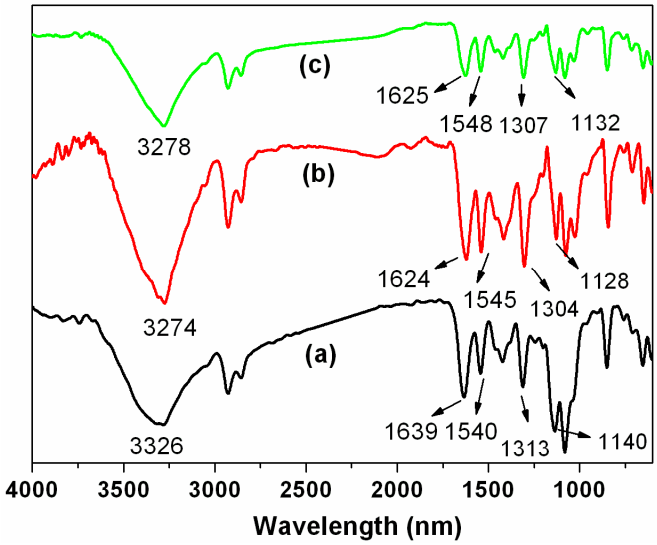

Figure S21. FTIR spectra of (a) 8 mM **P7** in DMF solution/sol and (b) **P7**/ethanol and (c) **P7**/acetonitrile xerogels (initial [**P7**] = 2%).

16. ^{1}H NMR spectra of P7 in DMSO-d_6

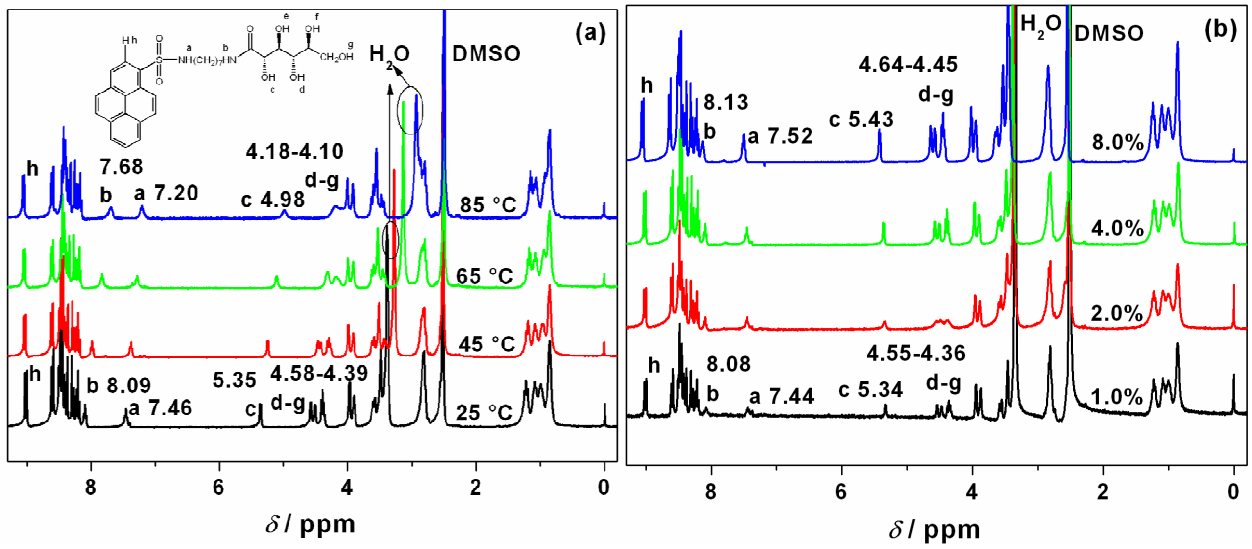

Figure S22. ^{1}H NMR spectra of **P7** in DMSO-d_6: (a) temperature dependence at 4.0%; (b) concentration dependence at 25 °C. The peaks at 3.39 ppm at 25 °C and 2.93 ppm at 85 °C in (a) and 3.33 ppm at 1.0% and 3.45 ppm at 8.0% in (b) are due to protons in water of the DMSO-d_6 solvent.

17. Solubility data for 2.5% P7 in neat liquids represented in Hansen space with spheres

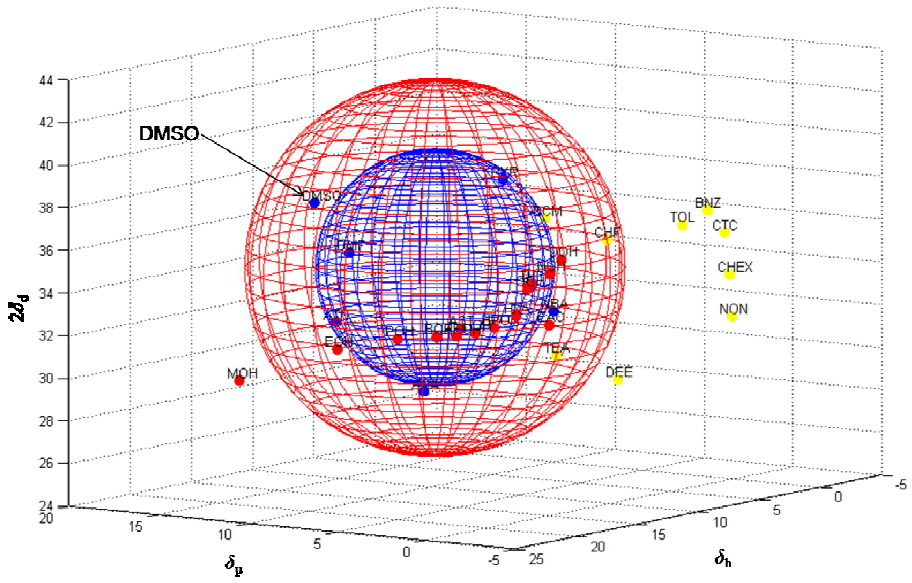

Figure S23. Solubility data for 2.5% **P7** in neat liquids represented in Hansen space with spheres. Blue (soluble), red (gel), and yellow (insoluble). For the sake of clarity, no yellow sphere is drawn. All points outside the red sphere are expected to be insoluble.

18. Rheology studies

Table S4. *G*' and *G*" values and *G*′/*G*″ ratios at stress = 10 Pa, and yield stress of 2% **P3-P8** in 1-decanol gels at 20 °C.

Pn	*G*′ (Pa)	*G*″ (Pa)	*G*′/*G*″	Yield stress (Pa)
P3	134000 ± 8000[a]	12070 ± 1070	11.1 ± 0.3	4190 ± 150
P4	1430 ± 130	330 ± 30	4.3 ± 0.1	30 ± 3
P6	20370 ± 1730	2590 ± 280	7.9 ± 0.2	40 ± 5
P7	67780 ± 3570	7830 ± 520	8.7 ± 0.2	1410 ± 80
P8	61320 ± 1300	6620 ± 460	9.3 ± 0.2	1260 ± 60

[a] Deviations are based on averages of 3 runs with different aliquots.

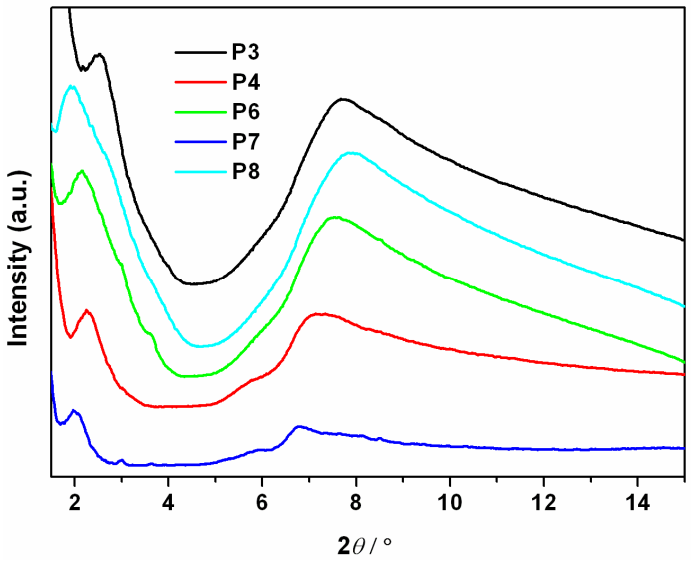

Figure S24. X-ray diffraction patterns of 10% **Pn** (Series B) in 1-decanol after subtracting empirically the amorphous scattering of the 1-decanol liquid from the total gel diffractograms.

Table S5. The values of 2θ and their corresponding d values of the diffraction peaks of gels of 10% **Pn** in 1-decanol.

Pn	2θ (°)	d (nm)
P3	2.52, 7.76	3.5, 1.14
P4	2.25, 7.14	3.92, 1.24
P6	2.15, 3.00, 3.67, 7.47	4.10, 2.94, 2.40, 1.18
P7	1.97, 3.01, 3.64, 6.76	4.48, 2.93, 2.42, 1.31
P8	1.90, 7.85	4.64, 1.12

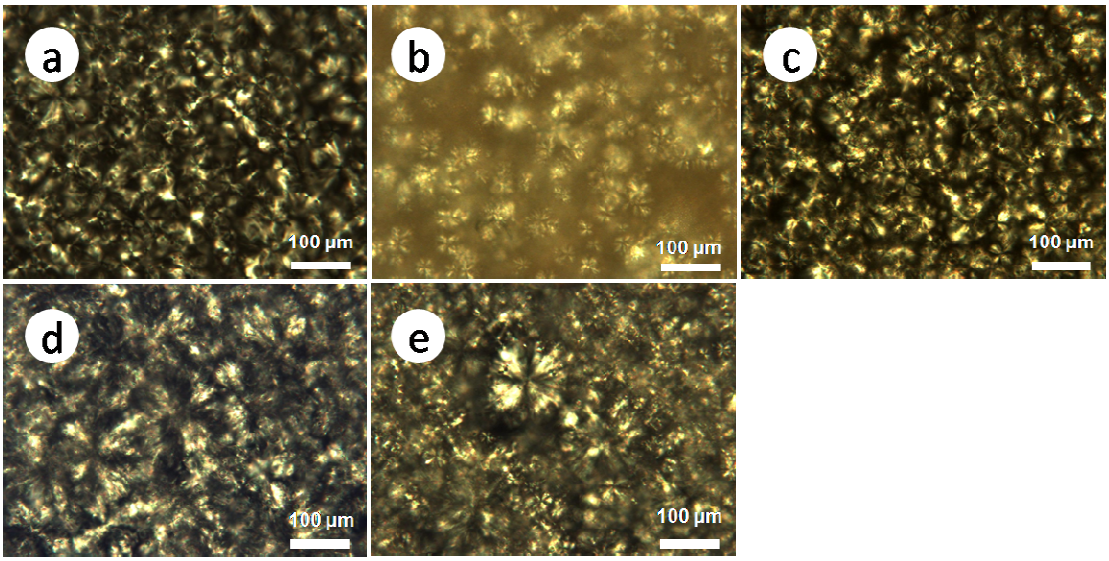

Figure S25. Polarizing optical micrographs of 2% **P3** (a)**, P4** (b)**, P6** (c)**, P7** (d) and **P8** (e) in 1-decanol.

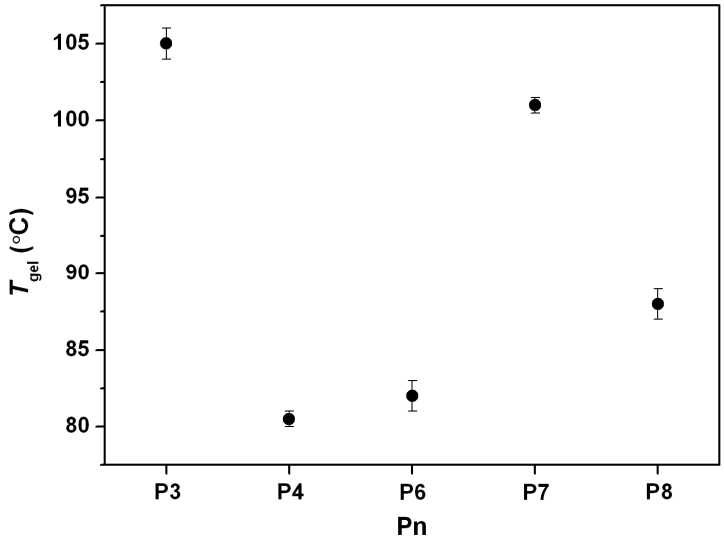

Figure S26. Plot of T_{gel} of 2% **Pn** in 1-decanol gels. Temperature ranges (vertical bars) refer to when the initial and final portions of a gel sample fell on being heated slowly.

Table S6. *G*' and *G*" values and *G*′/*G*″ ratios at stress = 10 Pa, and yield stress of **P7** in 1-decanol gels at different concentrations at 20°C.

P7 (%)	G′ (Pa)	G″ (Pa)	G′/G″	Yield stress (Pa)
0.5	6 ± 1[a]	7 ± 1	0.9 ± 0.1	8 ± 1
0.8	2300 ± 190	580 ± 75	4.0 ± 0.2	60 ± 7
1.0	17330 ± 1210	3420 ± 370	5.1 ± 0.2	800 ± 60
2.0	67780 ± 3570	7830 ± 520	8.7 ± 0.2	1410 ± 80

[a] Deviations are based on averages of 3 runs with different aliquots.

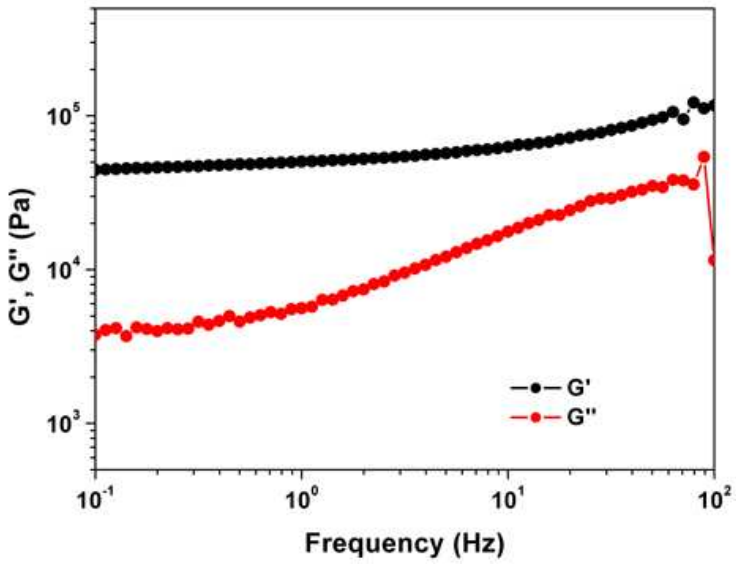

Figure S27. Log-log frequency sweep (shear stress = 12 Pa) for a gel of 2.0% **P7** in 1-decanol at 20 °C.

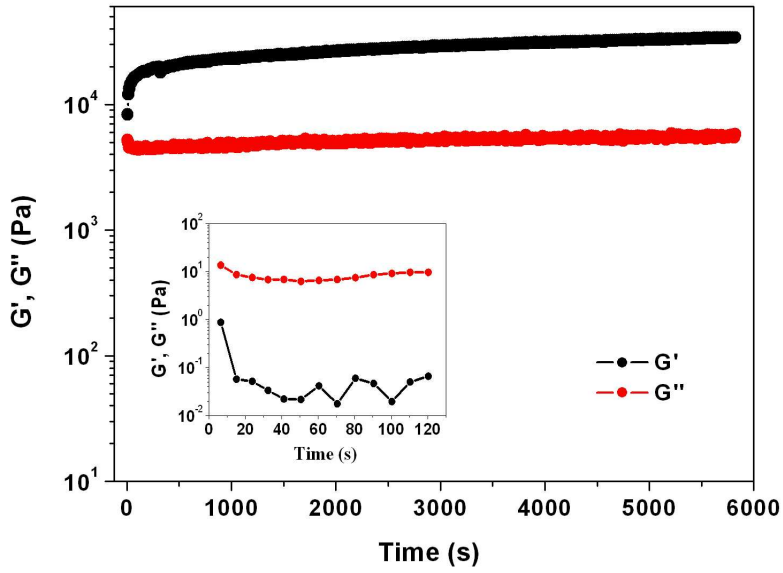

Figure S28. Evolution of *G′* and *G″* of a 2.0% **P7** in 1-decanol gel as a function of time after an initial shear stress of 1680 Pa had been applied for 2 min at 20 °C (as shown in the inset). The recovery was monitored at an applied stress of 1 Pa, and the time axis starts after the end of the destructive shear.

References

(1) Ezzell, S. A.; McCormick, C. L. Water-soluble copolymers. 39. Synthesis and solution properties of associative acrylamido copolymers with pyrenesulfonamide fluorescence labels. *Macromolecules* **1992**, *25*, 1881-1886.

(2) Yan, N.; He, G.; Zhang, H. L.; Ding, L. P.; Fang, Y. Glucose-based fluorescent low-molecular mass compounds: creation of simple and versatile supramolecular gelators. *Langmuir* **2010**, *26*, 5909-5917.

(3) Yang, M.; Yan, N.; He, G.; Liu, T.; Fang, Y. Synthesis and gelation behavior of a pyrene-containing glucose derivative. *Acta. Phys. -Chim. Sin.* **2009**, *25*, 1040-1046.